Gondwana Research 138 (2025) 168–185

Contents lists available at ScienceDirect

Gondwana Research

journal homepage: www.elsevier.com/locate/gr

The impact of Pangean subducted oceans on mantle dynamics: Passive piles and the positioning of deep mantle plumes

Philip J. Heron [a,*], Juliane Dannberg [b,g], Rene Gassmöller [b,g], Grace E. Shephard [c,d], Jeroen van Hunen [e], Russell N. Pysklywec [f]

[a] University of Toronto Scarborough, Dept of Physical and Environmental Sciences, Toronto ON, Canada
[b] University of Florida, Gainesville, FL 32611, United States
[c] University of Oslo, Centre for Planetary Habitability (PHAB), Department of Geosciences, Oslo, Norway
[d] Australian National University, Research School of Earth Sciences, Canberra, ACT, Australia
[e] Durham University, Dept of Earth Sciences, Durham, UK
[f] University of Toronto, Dept of Earth Sciences, Toronto ON, Canada
[g] GEOMAR Helmholtz Centre for Ocean Research Kiel, Kiel, Germany

ARTICLE INFO

Handling Editor: J. Meert

Keywords:
Mantle convection
LLSVP
Plume
Mantle dynamics
Subduction

ABSTRACT

Seismic imaging of the Earth's interior reveals plumes originating from relatively hot regions of the lowermost mantle, surrounded by cooler material thought to be remnants of ancient subducted oceans. Currently, there is no clear consensus on the internal composition of the hot regions, with end-member conditions being that they are thermo-chemical in nature or purely thermal plume clusters. Previous modelling studies have shown a range of scenarios where deep chemical heterogenities or purely thermal anomalies are essential in developing appropriate present-day mantle dynamics. Here, we add to this discussion by quantifying the location of rising mantle plumes using numerical 3-D global mantle convection models constrained by 410 million years of palaeo-ocean evolution (encompassing the formation and breakup of supercontinent Pangea). Our study compares numerical simulations with purely thermal convection to those where a deep thermo-chemical anomaly is laterally mobile. The results show that models both with and without large-scale chemical heterogeneities can generate appropriate present-day plume dynamics, which illustrate the power of sinking ocean plates to stir mantle ow and control the thermal evolution of the mantle. Our models add to the discussion on bottom-up and top-down mantle dynamics, indicating the difficulty in unravelling the processes using numerical models alone.

1. Introduction

Large structures of low seismic velocities (the Large Low Shear Velocity Provinces, or LLSVPs) observed in the lower mantle in seismic tomography studies and interpreted as regions of elevated temperatures, appear to play a defining role in the origins and positioning of mantle plumes (Steinberger, 2000; McNamara and Zhong, 2005; Torsvik et al., 2006; Cottaar and Lekic, 2016; French and Romanowicz, 2015). Although the fundamentals of composition, origin, and dynamics of LLSVPs are still being debated (e.g., Torsvik et al., 2010; Deschamps et al., 2012; Davies et al., 2012; Koelemeijer et al., 2017; Zaroli et al., 2017; Bull et al., 2014; Flament et al., 2022), there is growing agreement (Garnero et al., 2016) that plumes may form in some way from these regions (Fig. 1). The formation of plumes can influence supercontinent dispersal, leading to a further repositioning of subduction zones and a change in mantle ow (Burov and Cloetingh, 2010; van Hinsbergen et al., 2011; Cloetingh et al., 2021).

The nature of LLSVPs has been at the centre of plume generation discussions for nearly two decades (McNamara and Zhong, 2005; Torsvik et al., 2006; Davies and Davies, 2009; Davies et al., 2012; Bull et al., 2014; Flament et al., 2022). Geochemical data from surface melts indicate the presence of chemical mantle reservoirs (Allègre, 1982; White, 1985; Allègre and Turcotte, 1986; Carlson, 1994; Tackley, 2000, 2007; Gonnermann and Mukhopadhyay, 2007, 2009; Jackson et al., 2014; White, 2015), with hotspot-derived melts associated with plumes consistently showing a different mantle source composition than mid-ocean ridge basalts. Evidence suggests that spatial geochemical patterns at oceanic islands reflect preferential sampling of a distinct source

* Corresponding author.
E-mail address: philip.heron@utoronto.ca (P.J. Heron).

https://doi.org/10.1016/j.gr.2024.10.007
Received 5 February 2024; Received in revised form 17 September 2024; Accepted 17 October 2024
Available online 23 October 2024

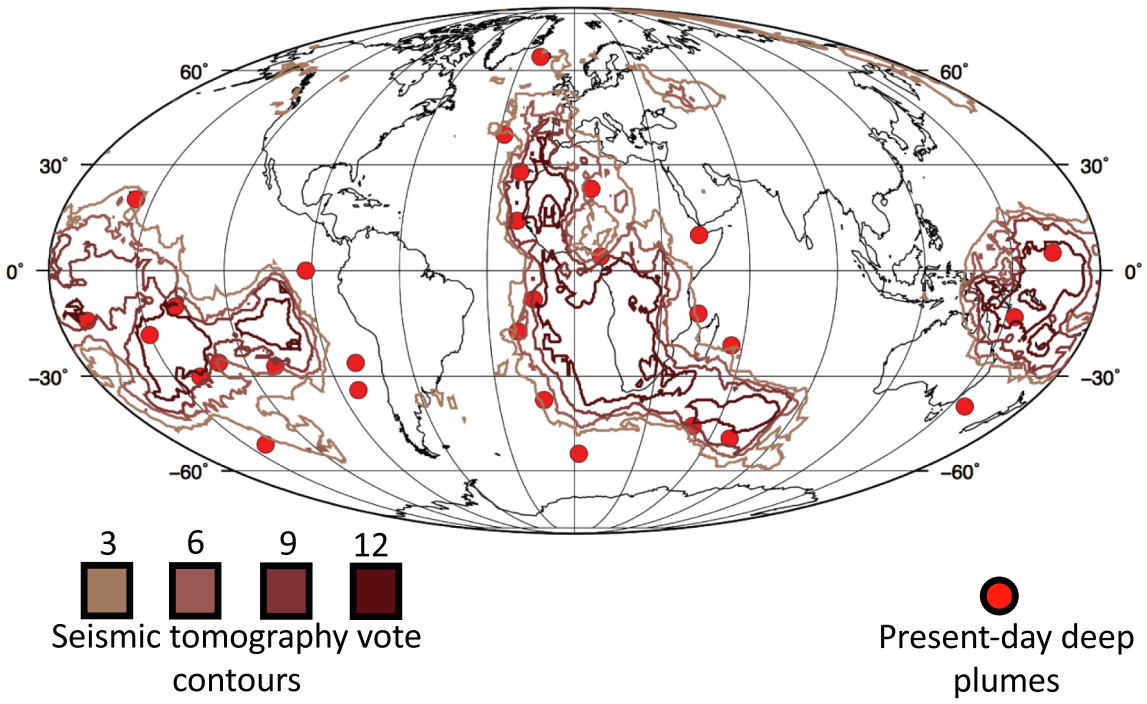

Fig. 1. Present-day mantle features. Position of low velocity provinces (LLSVPs) at 2800 km depth alongside the approximate locations for present-day deep mantle plumes and hotspots (Steinberger, 2000; French and Romanowicz, 2015; Whittaker et al., 2015) (Table 3). The low velocity regions are contours where 3, 6, 9, and 12 (out of 14) seismic tomography models agree that there are slow anomalies (Shephard et al., 2017).

of deep mantle material originating from the LLSVPs (Weis et al., 2011; Farnetani et al., 2012; Williams et al., 2015). These observations have led to the idea that the LLSVPs may be 'thermo-chemical' piles of material with a different composition than the average mantle.

The fundamental composition and structure of the two deep seismic tomography anomalies is still not clear. The LLSVPs have been characterized by higher than average densities through early tomographic normal mode data and the anti-correlation of bulk sound and shear wave anomalies (Su and Dziewonski, 1997; Ishii, 1999; Karato and Karki, 2001; Masters and Gubbins, 2003; Simmons et al., 2010; Trampert, 2004; Koelemeijer et al., 2012). Analysis using tidal tomography has also inferred structures of increased density in the lower mantle (Lau et al., 2017). However, work using Stoneley mode data offered an opposing view which indicated the potential for lighter material (Koelemeijer et al., 2017) or a layer with density stratifications (Robson et al., 2021). Compositional heterogeneities and/or a phase change to post-perovskite could both fit seismic observations in the lowermost mantle (Trampert et al., 2001; Deschamps and Trampert, 2003) and the possibility that LLSVPs are purely thermal anomalies has also been put forward (Schubert et al., 2004).

Previous geodynamic modelling studies have indicated that a thermo-chemical nature of the deep mantle material is essential in producing appropriate present-day plume positions (Steinberger and Torsvik, 2012; Hassan et al., 2015; Li and Zhong, 2017; Bull et al., 2014). However, the rheological nature of LLSVPs and their role in mantle dynamics are still being debated (Davies and Davies, 2009; Torsvik et al., 2010; Burke, 2011; Davies et al., 2012; Bower et al., 2013; Bull et al., 2014; Zhong and Rudolph, 2015; Zhong and Liu, 2016; Zaroli et al., 2017; Heyn et al., 2018, 2020; Flament et al., 2022; Heron et al., 2021, 2024), with some studies indicating the potential for purely thermal deep mantle dynamics to also be in keeping with observations (e.g., Davies et al., 2015; Hassan et al., 2015). Important open questions remain: Are LLSVPs thermal plume clusters or dense, stable thermo-chemical piles, or a mixture of the two (e.g., Davaille and Romanowicz, 2020)? Have LLSVPs been present and stable for most of the Earth's history? And do they control the location of rising plumes? A key component to answering these questions lies in understanding the mechanisms that cause plumes to rise in the locations where hotspots are observed on Earth today.

To study mantle dynamics, we use 3-D thermo-chemical global mantle convection experiments that take into account palaeo-subduction history from 410 Ma to the present day (Matthews et al., 2016) which incorporates plate reconstructions models of the Paleozoic (Domeier and Torsvik, 2014) and Mesozoic-Cenozoic (Müller et al., 2016). We then compare the results at the end of the model run to observations of LLSVP shape (Cottaar and Lekic, 2016; French and Romanowicz, 2015; Shephard et al., 2017) and plume positions (Steinberger, 2000; French and Romanowicz, 2015; Whittaker et al., 2015). By applying different subduction histories as a time-dependent boundary condition to our models (e.g., McNamara and Zhong, 2005; Zhang et al., 2010; Steinberger and Torsvik, 2012; Davies et al., 2012; Bower et al., 2013; Bull et al., 2014; Hassan et al., 2015, 2016; Flament et al., 2017; Li and Zhong, 2017; Zhang and Li, 2018; Flament et al., 2022), we gain insights on the role of subducted slabs in shaping the LLSVPs and triggering the ascent of mantle plumes. In addition, we systematically vary the thickness of a compositional heterogeneity in the lowermost mantle, thereby controlling the dynamics of the hot regions that represent the LLSVPs. This allows us to evaluate which of the proposed end-member scenarios – an anomaly that is purely thermal or one that is thermo-chemical – is supported by the observations.

In this study, we incorporate subduction history encompassing the formation and breakup of the supercontinent Pangea. The life-cycle of a supercontinent has a dramatic impact on mantle dynamics (Santosh et al., 2009; Santosh, 2010; Yoshida and Santosh, 2011; Li et al., 2008; Li and Zhong, 2009; Heron, 2018), and we show that the subduction history affects plume and LLSVP formation on different time scales (e.g., Heyn et al., 2020; Cao et al., 2021a,b; Flament et al., 2022). In our model results, we discover the mantle circulation dynamics that connect past plate motions and ocean island volcanism (e.g., hotspots, Fig. 1). We show that the two opposing hypotheses – plume clusters and thermo-chemical piles – are both able to reproduce the observed positions of present-day hotspots equally well, highlighting the importance of

Table 1
Modelling parameters.

Symbol	Variable	Value
η	Dynamic viscosity	literature (Steinberger and Calderwood, 2006)
ρ	Density	PerpleX (Connolly, 2009; Stixrude and Lithgow-Bertelloni, 2011; Xu et al., 2008)
g	Gravitational acceleration	9.81 $m.s^{-1}$
C_p	Specific heat capacity	PerpleX (Connolly, 2009; Stixrude and Lithgow-Bertelloni, 2011; Xu et al., 2008)
k	Thermal conductivity	4.7 $W.m^{-1}.K^{-1}$
H	Radiogenic heat production	6×10^{-12} $W.kg^{-1}$
α	Thermal expansivity	PerpleX (Connolly, 2009; Stixrude and Lithgow-Bertelloni, 2011; Xu et al., 2008)

ancient subducted oceans in stirring the convecting mantle. We finish our discussion by highlighting potential next steps and emphasizing the significant potential of coupling studies of mantle dynamics and plate reconstructions.

2. Material and methods

2.1. Model setup

Computations were done using the ASPECT code (Kronbichler et al., 2012; Heister et al., 2017). ASPECT solves the following set of equations for compressible convection in the Earth's mantle, describing the mass, force and energy balance (taking into account adiabatic heating, shear heating and radiogenic heat production), and the transport of chemical composition:

$$-\nabla\cdot(2\eta\dot{\varepsilon})+\nabla p=\rho\mathbf{g}, \tag{1}$$

$$\nabla\cdot(\rho\mathbf{u})=0, \tag{2}$$

$$\rho C_p\left(\frac{\partial T}{\partial t}+\mathbf{u}\cdot\nabla T\right)-\nabla\cdot k\nabla T=\rho H+2\eta(\dot{\varepsilon}:\dot{\varepsilon})+\alpha T(\mathbf{u}\cdot\nabla p), \tag{3}$$

$$\frac{\partial C}{\partial t}+\mathbf{u}\cdot\nabla C=0. \tag{4}$$

The equations are solved for velocity **u**, pressure p, temperature T and chemical composition C. η is the viscosity, $\dot{\varepsilon}=\frac{1}{2}\left(\nabla\boldsymbol{u}+\nabla\boldsymbol{u}^{T}\right)-\frac{1}{3}(\nabla\bullet\boldsymbol{u})\delta_{ij}$ is the deviatoric strain rate, **g** is the gravitational acceleration, ρ is the density, C_p is the specific heat capacity (at constant pressure), k is the thermal conductivity, H is the radiogenic heat production, and α is the thermal expansivity.

We use the global model setup (Heister et al., 2017) employed in a previous studies (Dannberg and Gassmöller, 2018; Heron et al., 2021, 2024; Dannberg et al., 2023). Here, our plate reconstruction (Matthews et al., 2016), which provides velocity boundary conditions at the surface of the model, extends back in time 410 million years.

As in a previous study (Dannberg and Gassmöller, 2018), we assume an average mantle composition of 82 % harzburgite and 18 % recycled oceanic crust (Xu et al., 2008) and compute the material properties ρ, α and C_p using PerpleX (Connolly, 2009) and a mineral physics database (Stixrude and Lithgow-Bertelloni, 2011). Accordingly, the effects of phase transitions are included, with thermal expansivity and specific heat approximating the corresponding latent heat release (Nakagawa et al., 2009). Select model parameters are given in Table 1, and the initial radial profiles of temperature- and depth-dependent material properties are plotted in Fig. 2. The viscosity law used here produces very strong lateral and vertical viscosity variations over the temperature range appropriate for Earth (Fig. 2). We limit the viscosity range to ~four orders of magnitude to reduce the computation time and make model runs feasible ($1 \times 10^{19} - 5 \times 10^{23}$ Pa s).

Our focus is on deep mantle heterogeneity and its impact on mantle dynamics. Therefore, we vary the amount of dense recycled oceanic crust material (e.g., the volume of thermo-chemical piles) present in the mantle. The initial thickness of this layer is varied between 0 km (purely thermal model) and 300 km for different model runs (Table 2; Model0, Model50, Model100, Model150, Model200, and Model300). However, in this study we do not vary the density of the deep mantle heterogeneity between model runs and keep the compositional buoyancy of the layer in comparison to the surrounding material the same for all experiments. Our core-mantle boundary temperature is 3700 K which corresponds to a buoyancy number for the thermo-chemical material of $B=\frac{\Delta\rho}{\alpha\rho\Delta T}\Delta^{\rho}=1.9$, where Δρ and Δ T are 2 % and 1284 K, respectively, and represent the contrast between the anomalously dense material and the average mantle composition at 2500 km.

Our numerical models have varying resolution as a function of both the large-scale mantle layering and smaller-scale mantle dynamics (see Fig. 2g). The minimum resolution in all models is approximately ~40 km, with ~2 million cells and ~40 million degrees of freedom at the end of each model run. We use second-order finite elements, leading to a

Table 2
List of models with corresponding initial thermo-chemical (TC) thickness, and plate reconstruction study.'Modi ed' refers to a 410 Myr reconstruction that uses Seton et al. (2012) 250 Ma to 90 Ma surface velocities for 410 Ma to 250 Ma, then repeats until present day.

Name	Initial TC	Plate reconstruction
Model 0	0 km	410 Ma Matthews et al. (2016)
Model50	50 km	410 Ma Matthews et al. (2016)
Model100	100 km	410 Ma Matthews et al. (2016)
Model150	150 km	410 Ma Matthews et al. (2016)
Model200	200 km	410 Ma Matthews et al. (2016)
Model300	300 km	410 Ma Matthews et al. (2016)
Model200s	200 km	410 Ma Modified Seton et al. (2012)

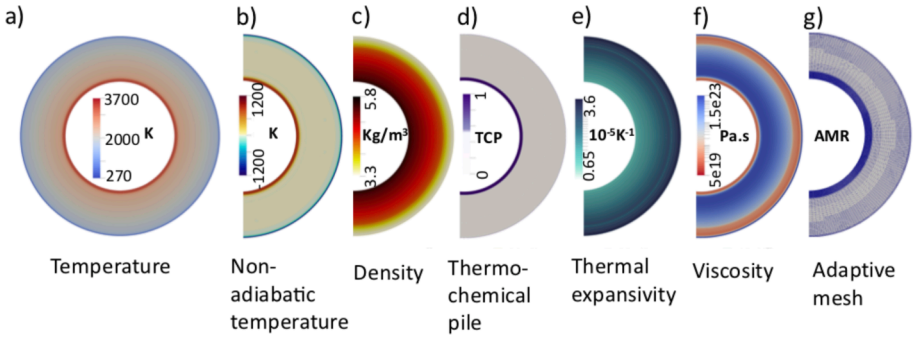

Fig. 2. Initial conditions of the models (at 0 Myr/410 Ma), showing cross-sectional views of (a) temperature, (b) non-adiabatic (excess) temperature, (c) density, (d) initial thermo-chemical pile thickness (200 km in Model200 shown here), (e) variable thermal expansivity, (f) viscosity, (g) the initial adaptive mesh.

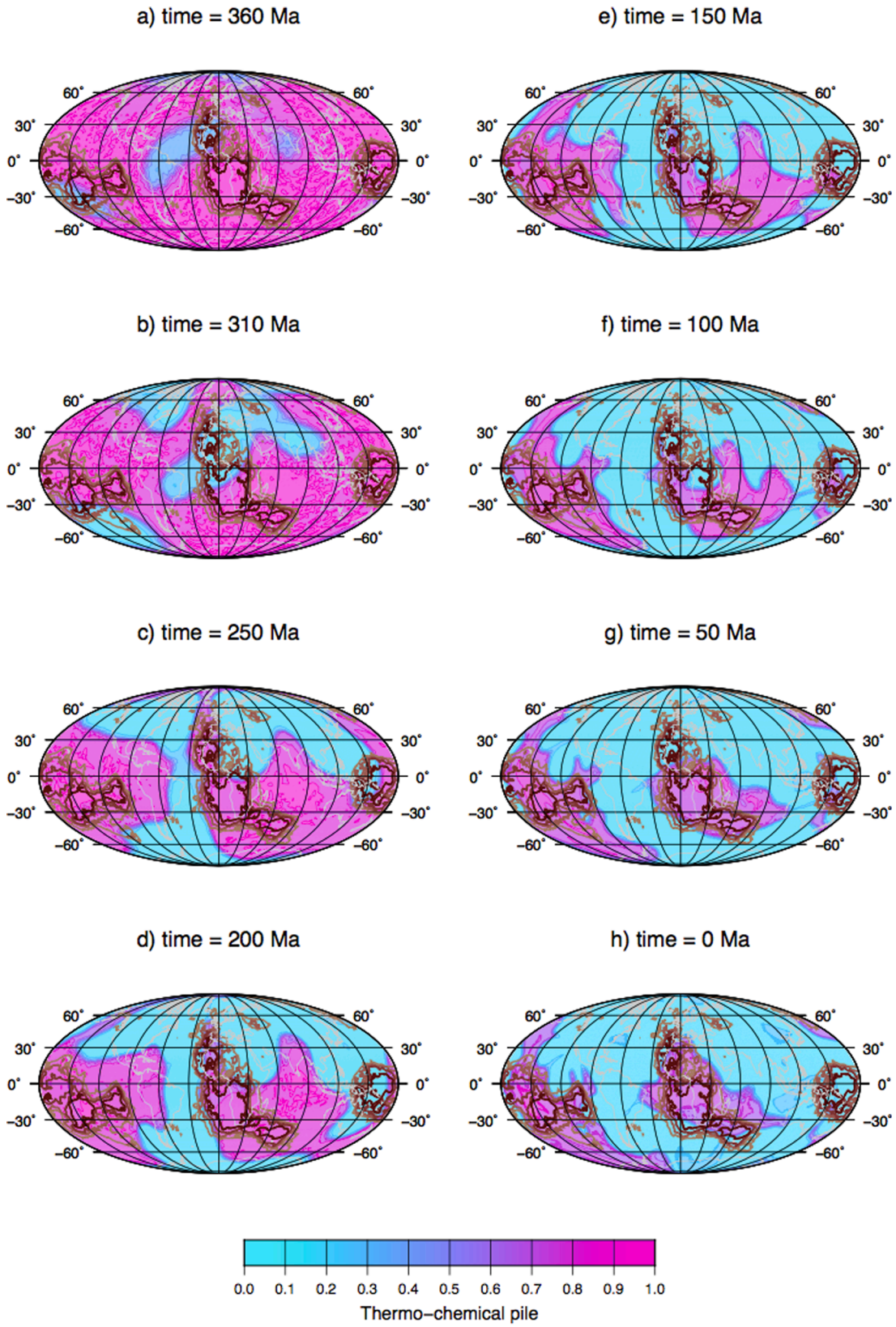

Fig. 3. Evolution of chemical heterogeneities in Model200 from 410 Ma to present day. The snapshots (a)-(h) show the proportion of anomalous, dense material in a spherical slice at 2800 km depth, illustrating how the material evolves from a layer with uniform thickness into a thermo-chemical pile. Brown contours indicate observed low seismic velocity anomalies as in Fig. 1.

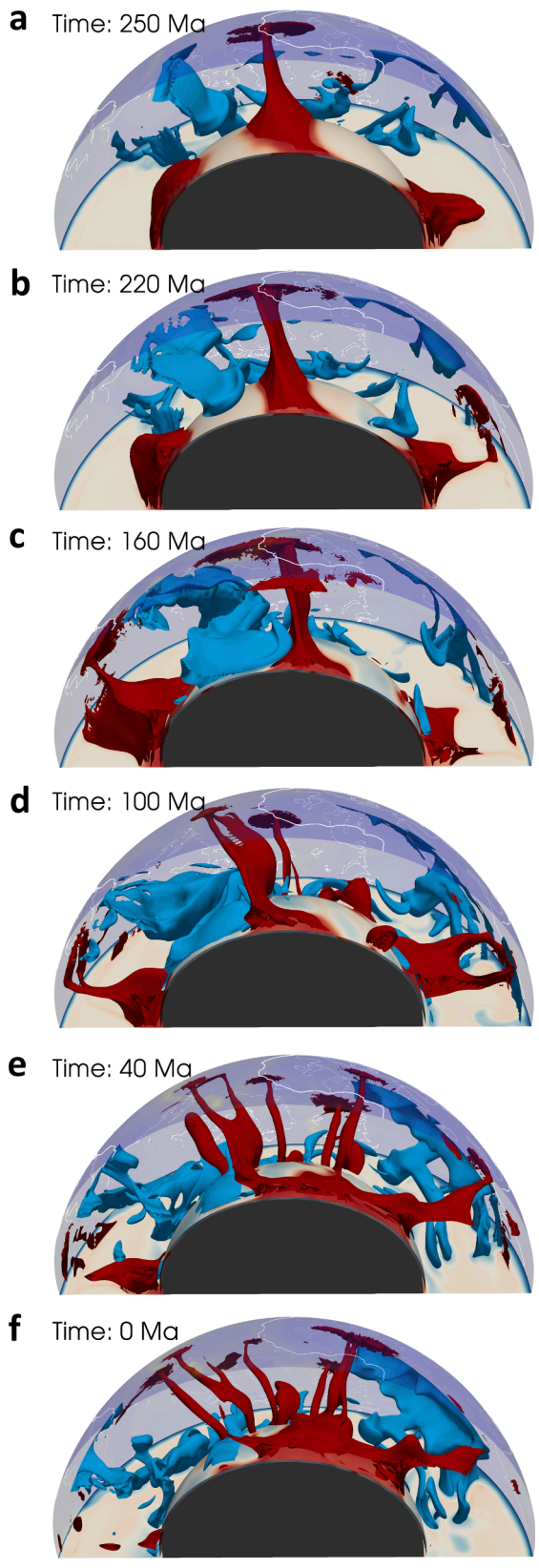

Fig. 4. Thermo-chemical piles in this study are passive in mantle dynamics. Evolution of the hot and cold anomalies under the African northern hemisphere from 250 Ma (a) to present-day (f) for Model200. Excess mantle temperature anomaly contoured surfaces are given for warm (300 K, red) and cold (−500 K, blue) regions. (For interpretation of the references to colour in this figure legend, the reader is referred to the web version of this article.)

Table 3
Approximate locations of present-day plume and hotspots as used as a reference in this study, based on data from French and Romanowicz (2015), Whittaker et al. (2015), and Steinberger (2000). We compare these points to our model plume positions calculated at 700 km below the surface.

#	Latitude	Longitude	Notes
1	−14	−170	Samoa
2	20	−156	Hawaii
3	−18	−150	Tahiti/Society
4	−51	−141	Louisville
5	−30	−140	Cook
6	−10	−138	Marquesas
7	−26	−130	Pitcairn
8	−27	−110	Easter
9	0	−92	Galapagos
10	−34	−83	Juan Fernandez
11	−26	−80	San Feliz
12	39	−28	Azores
13	28	−20	Canary
14	14	−20	Cape Verde
15	65	−20	Iceland
16	−17	−20	St Helena
17	−8	−14	Ascension
18	−37	−12	Tristan
19	−54	2	Bouvet
20	23	6	Hoggar
21	4	9	Cameroon
22	10	43	Afar
23	−12	43	Comores
24	−45	50	Crozet
25	−21	56	Renuion
26	−49	69	Kerguelen
27	−13	153	Tasmanid
28	−39	156	Caroline
29	5	164	Indonesia

Table 4
Database of large igneous province positions (Torsvik et al., 2006, 2008) from 251 Ma to 99 Ma.

Age (Ma)	Latitude	Longitude	LIP Name
251	57.7	54.7	Siberian Traps
200	2.5	341.9	Central Atlantic Magmatic Province (CAMP)
182	−44.6	2.8	Karroo Basalts
147	−4	219	Shatsky Rise
145	−26.9	244.3	Megallan Rise
132	−55.3	81.6	Bunbury Basalts
132	−34.9	350.6	Parana-Etendeka
125	−54.7	5.9	Maud Rise
123	−34.5	264.5	Manihiki Plateau
121	38.2	219.7	Ontong Java Plateay
118	−41.6	67	Rajhmahal Traps
114	−52.3	64.9	South Kerguelen
111	−26.4	222	Naura Basalts
100	−45.4	63.3	Central Kerguelen
99	2.6	225.4	Hess Rise

minimum distance between quadrature points of 20 km. In terms of mantle layering, we apply the highest resolution grid to the bottom 390 km of our model (to capture the thermal instabilities of the core-mantle boundary) and the second highest resolution to the top 80 km (to capture the evolving surface conditions). Between 80 km and 660 km depth is a range with the third highest resolution, and the middle of the mantle (660–2500 km) has the lowest resolution in all the models (Fig. 2g). The spatial resolution in all models is further controlled by refining the mesh in regions of gradients in composition, viscosity, or temperature to capture any smaller scale features, updating every 3 timesteps. The full input files can be found in the link in the Data Availability section.

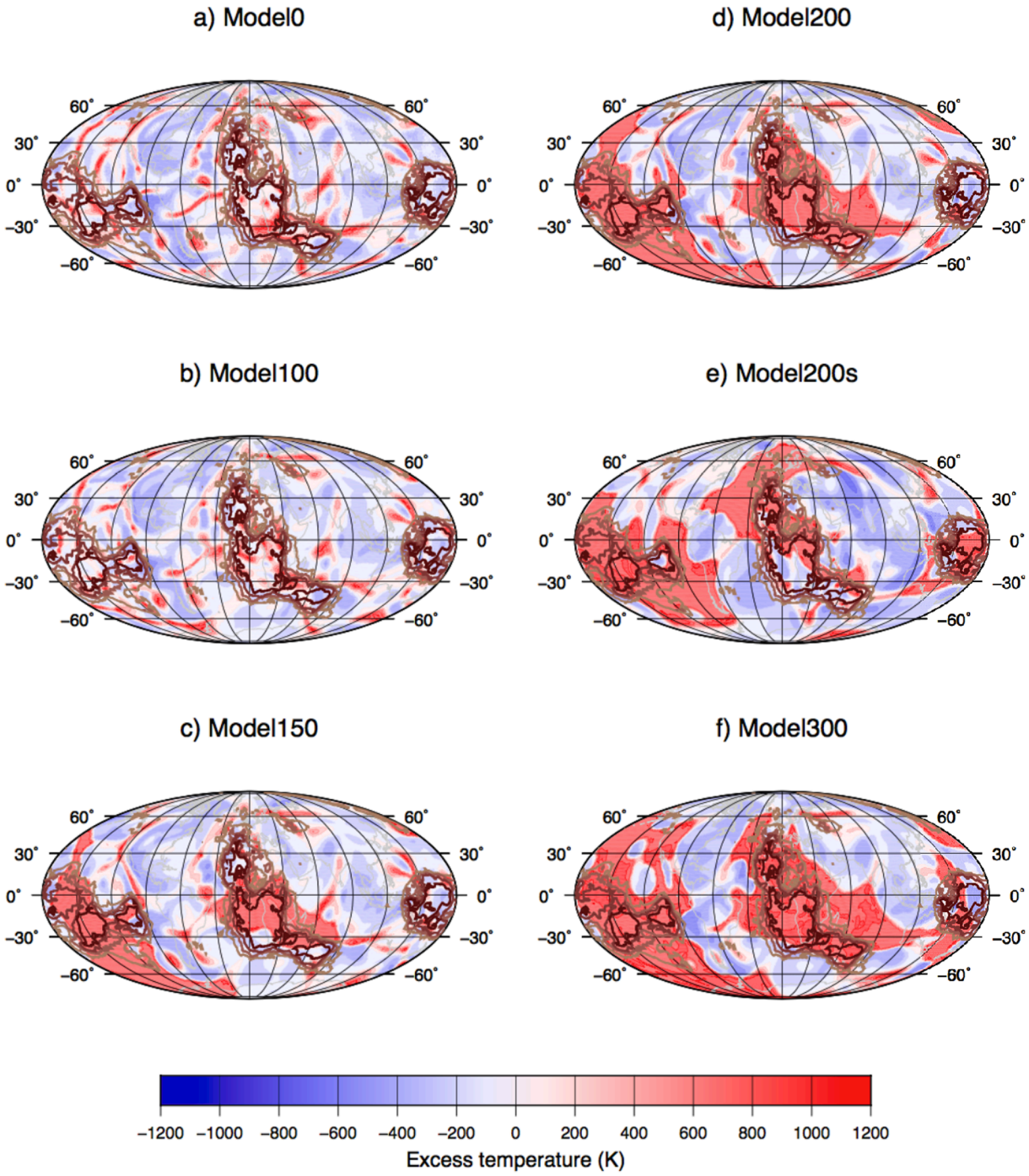

Fig. 5. Differences in core-mantle boundary temperature and dynamics between models with varying amount of chemical hetero- geneity. Present-day (0 Ma) excess temperature in 2800 km depth for (a) Model0, (b) Model100, (c) Model150, (d) Model200, (e) Model200s, and (f) Model300. Brown contours indicate low seismic velocity anomalies as in Fig. 1.

2.2. *Model evolution*

Our models begin from an initial condition that has an average mantle temperature gradient and composition that is appropriate for the present-day mantle (Fig. 2) as applied by previous studies (e.g., Dannberg and Gassmöller, 2018; Zhang and Li, 2018). The initial mantle temperature is laterally homogeneous, following an adiabatic profile with thermal boundary layers at the top and bottom (Dannberg and Gassmöller, 2018). We fix the surface temperature to 273 K and core–mantle boundary temperature to 3700 K (Fig. 2). Although 3700 K is a higher temperature than used in some previous studies (Zhang and Li, 2018), it is well within the range of uncertainty for the exact present-day value (Nomura et al., 2014).

For our reference model presented here, a 200 km thick layer of anomalous, dense material is initially emplaced at the core-mantle boundary (Model200). In Model200, the subduction pattern during the formation and dispersal of the supercontinent Pangea shapes the hot thermo-chemical material into two distinct regions in roughly the same locations as the observed LLSVPs (e.g., Fig. 3). We herein refer to thermo-chemical piles from the numerical models as 'TCPs' and reserve the 'LLSVPs' for the seismically imaged structures to which TCPs are compared.

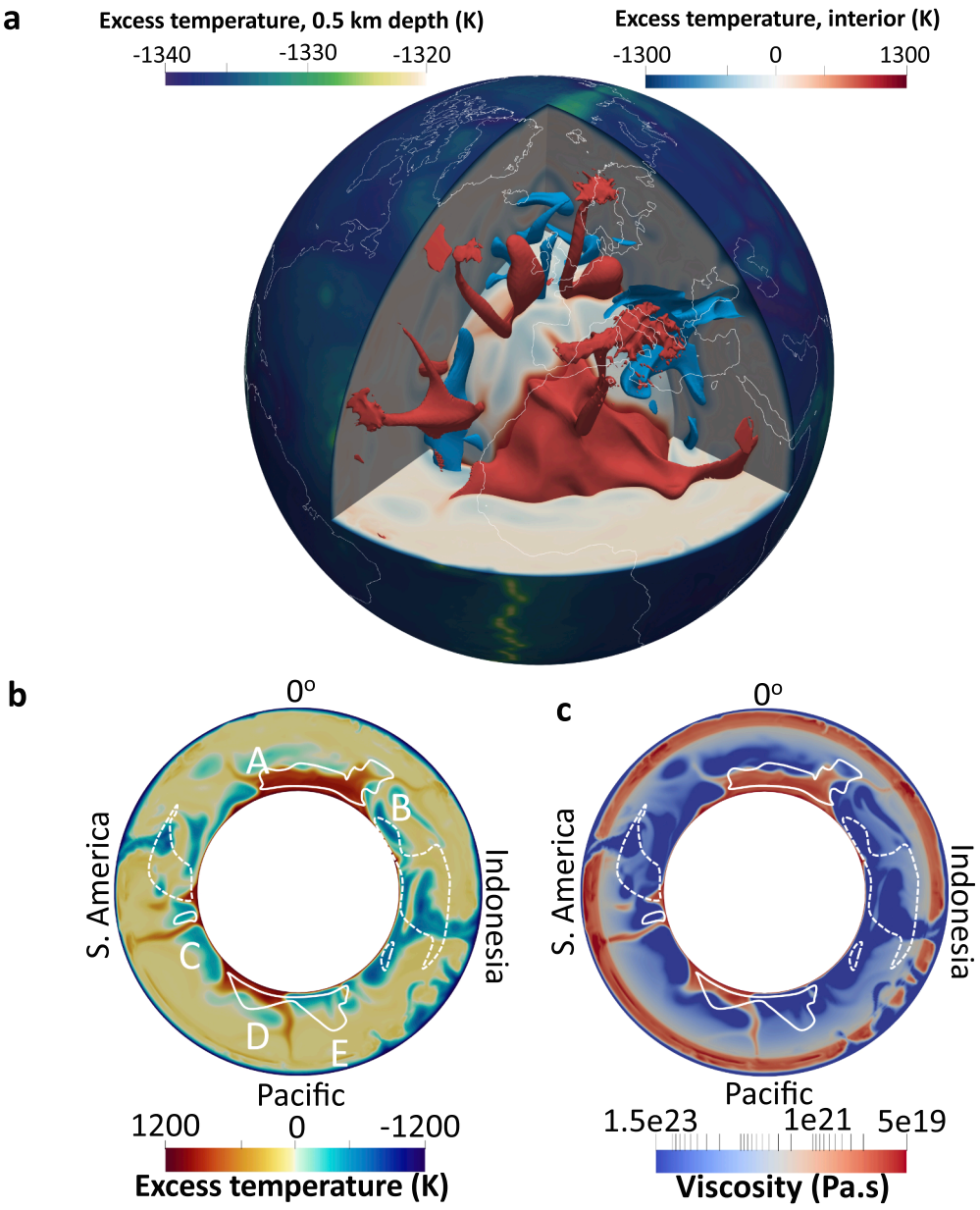

Fig. 6. Global mantle dynamics and temperature compared with seismic models. (a) A view into the mantle beneath the northern Atlantic and Europe for Model200. Excess mantle temperature anomaly contoured surfaces are given for warm (300 K, red) and cold (−500 K, blue) regions. (b) Excess temperature slice at the equator, and the corresponding viscosity distribution (c), with the outline of where four seismic tomography studies agree that there is a shear velocity anomaly (Cottaar and Lekic, 2016) shown by white solid (slow) and dashed (fast) lines. Key: A: steep western side of the African LLSVP; B: angled eastern flank of the African LLSVP; C: Galapagos plume position; D: eastern Pacific LLSVP pile; E: western Pacific LLSVP pile. (For interpretation of the references to colour in this figure legend, the reader is referred to the web version of this article.)

Fig. 4 shows the Model200 evolution of the hot (plume) and cold (downwelling) regions beneath Africa, highlighting a site of the former supercontinent Pangea. As our model TCP are mobile and can move with mantle flow (controlled here by Pangean subduction history), illustrating how deep mantle structure might have evolved over the past 250 Ma.

Using Model200 as a reference example, we take the mantle structure at 0 Ma and analyse the plume positions and thermo-chemical pile shape, as discussed in the following section.

2.3. Analysis of plume positions

To determine the locations of mantle plumes in our models, we define a plume as a positive temperature anomaly of at least 300 K excess temperature at a depth of 700 km. This depth was chosen in order to capture a first-order location of the conduit and to avoid complications associated with short-lived interactions between the plume head and upper mantle, such as entrainment or deflection by mantle wind.

These regions are then collated and spatially averaged into one data point for each plume. Table 3 and Fig. 1 show the hotspot catalogue we used as a comparison for the output of our geodynamic models. We quantify how well each model output fits this database of approximate present-day hotspots by using the following statistical method for comparing two sets of points.

First, we calculate the great-circle distance d between the model plumes and the hotspots in the database using the Spherical Law of Cosines:

$$d = arccos(sin(\varphi d_b)sin(\varphi_m) + (cos(\varphi d_b)cos(\varphi_m)cos(\lambda_m - \lambda d_b)))r_e \quad (5)$$

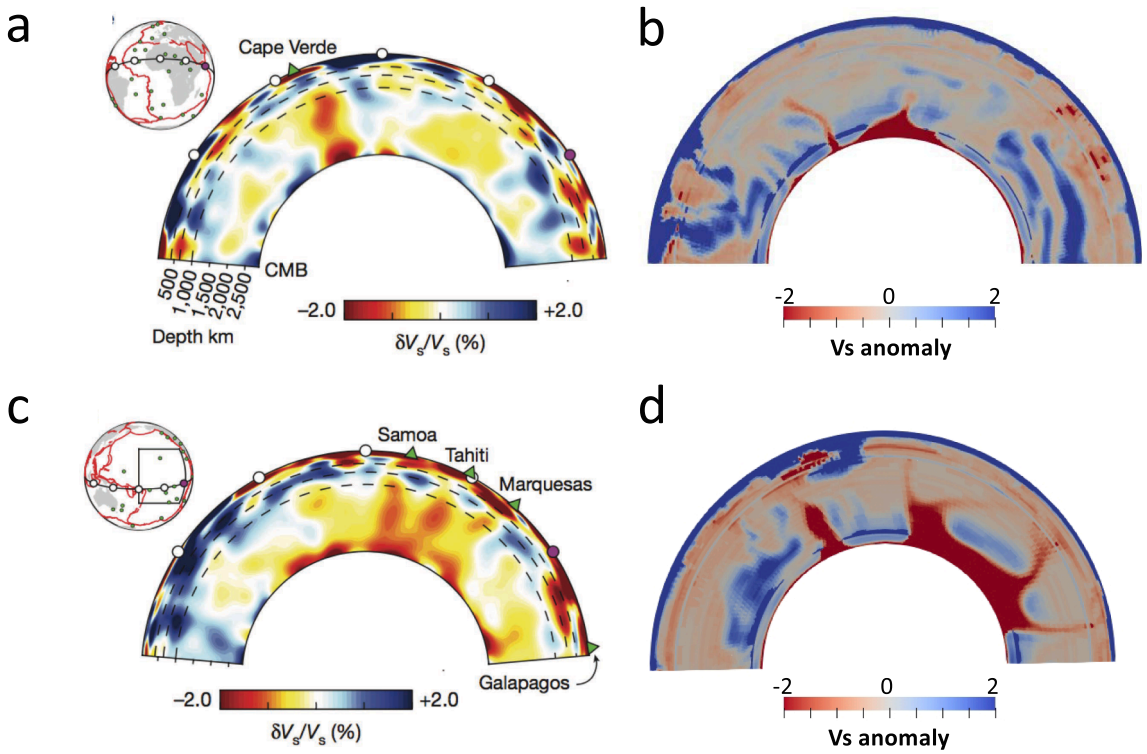

Fig. 7. Whole-mantle depth cross-section modified from French and Romanowicz (2015) of relative shear-velocity variations using model SEMUCB-WM1 (French and Romanowicz, 2014) near Cape Verde (a) and Marquesas (c), with the corresponding shear velocity anomaly output from Model200 shown in (b) and (d), respectively.

where φ and λ are the latitude and longitude, respectively, of the plume location in the model (m) and the position of the closest hotspot in the database (d_b), and r_e is the radius of the Earth.

To quantify how well each model fits the hotspot database, we use Equation (5) to compute the same statistics for 10,000 different models of 39 plumes generated at random latitudes φ_m and longitudes λ_m. We chose 39 plumes as that was the number generated by our reference Model200. These random runs allow us to compute percentiles indicating if the fit of a given model is better than, for example, the 15 %, 50 %, or 85 % of the best random sets of plume positions. Here, the 50 % percentile is equivalent to the average fit expected for a random plume distribution, and the 15 % and 85 % percentiles indicate approximately one standard deviation of this distribution.

3. Results

3.1. Mantle dynamics

We computed a suite of geodynamic models with varying amounts of chemical heterogeneity in the mantle in order to investigate a wide range of lower-mantle convection regimes and determine if any resemble today's mantle dynamics. As outlined in Table 2, we vary the initial thickness of the thermo-chemical layer at the base of the mantle.

All simulations where the initial dense layer is at least 150 km thick produce two distinct thermo-chemical piles (TCP, Fig. 5). Model50 and Model100 result in all the thermo-chemical material being entrained into the mantle during the simulation (shown by the lack of temperature clusters in Fig. 5b). Model0 (with no initial thermo-chemical pile) features purely thermal plume clusters at the model end (Fig. 5a).

Comparing the modelled African TCP with the shape of the African LLSVP, we find that Model200 has the most overlap (Fig. 5). The Pacific thermo-chemical pile also forms in the correct hemisphere in Model200, but the agreement with seismic tomography is generally not as good as in the African hemisphere. The modelled Pacific pile extends further north and south than the slow anomalies in tomography studies, and it is missing the western limb when compared with the LLSVP outline (Fig. 5d).

Fig. 6a shows the mantle under the northern Atlantic and Europe, indicating the excess temperature anomalies for upwelling plumes (red) and downwelling material (blue) for Model200. Comparing this model output at the equator to seismic tomography studies (Cottaar and Lekic, 2016) shows a number of similarities. Under Africa, our model TCP matches the shape of the LLSVP outline well, highlighting the steep western side (Ni et al., 2002) and angled eastern flank (A and B, Fig. 6b). In the Pacific hemisphere, our Model200 produces plume positions in the Galapagos (C, Fig. 6b) as well as a TCP in the eastern part of the Pacific LLSVP (D, Fig. 6b). However, our model misses the western flank of the Pacific LLSVP across the equator (E, Fig. 6b) as shown in Fig. 3h. Further direct comparisons with another seismic study (French and Romanowicz, 2015) are given in Fig. 7.

As mentioned above, models that begin with an initial condition where the thermo-chemical layer is less than 150 km thick do not produce two distinct piles at the present-day state. Given that the piles are mobile, meaning that they can be moved by the mantle flow, the thin starting layer ends up being mixed into the mantle for Model50 and Model100. However, in Fig. 8 we present a view into our models under the African northern hemisphere that shows similar mantle dynamics for the models both with (Model200) and without distinct piles (Model0 and Model100).

3.2. Present-day plume analysis

Direct comparison between tomography slices (Fig. 6b-c, Fig. 7) can give a first order interpretation of how well the models reproduce present-day mantle dynamics. However, another representation of model accuracy is to compare the difference between the approximate locations of present-day deep mantle plume and hotspots (Table 3) and the position of hot thermal anomalies in our models.

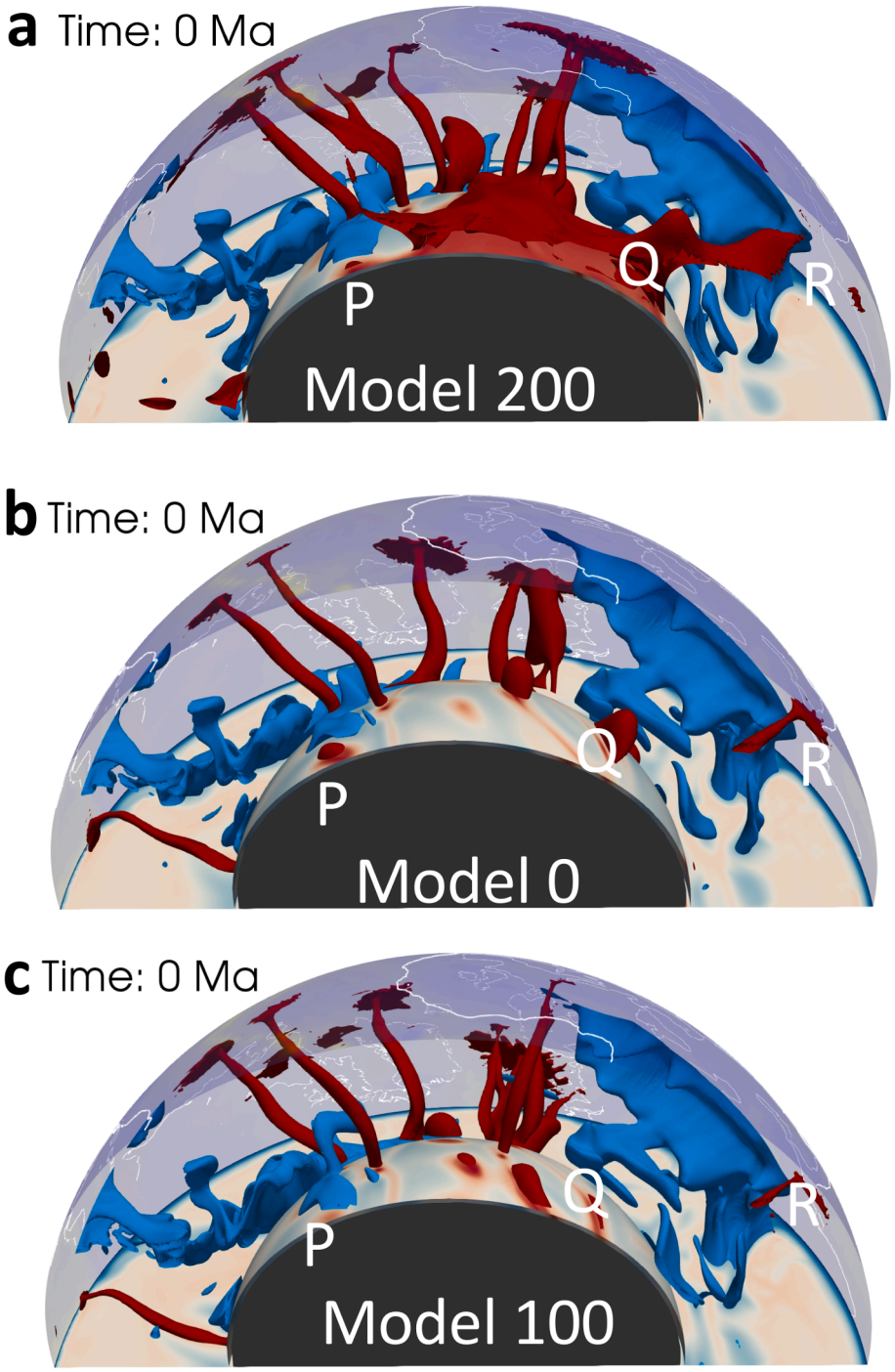

Fig. 8. Models with different amount of chemical heterogeneity can produce appropriate plume dynamics. Present-day snapshot of the hot and cold anomalies under the African northern hemisphere for (a) Model200, (b) Model0, and (c) Model100. Slice contours as Fig. 6. Markers P, Q, and R indicate equatorial plumes that could be linked to present-day hotspots St Helena, Comores, and Afar, respectively.

Fig. 9a illustrates the position of upwellings in Model200 at 700 km depth (green) alongside the approximate present-day plume and hotspot locations (Table 3) (red). The plume positions in our model do not appear to be randomly distributed, with upwellings forming close to the upwards projected margins of the LLSVPs in the African domain.

In the Pacific, a number of Model200 plumes form close to edges of the LLSVPs. Interestingly, this occurs in the western limb of the Pacific LLSVP even though there is no modelled thermo-chemical pile in that position (Fig. 3h). A number of Model200 plumes form within 1000 km of the Azores, Afar, Comores, St Helena, San Felix, Galapagos, Easter, and Pitcairn plumes (markers G to N in Fig. 9a, respectively). Furthermore, a deep mantle plume is positioned at the Indonesia site (marker O, Fig. 9a) where a previous study (French and Romanowicz, 2015) had imaged a plume despite no corresponding surface hotspot.

Fig. 9a also shows the positioning of plumes generated from a model that does not feature any thermo-chemical piles (Model0, blue circles). There is a similarity between the blue and green plume positions despite different lowermost mantle structure.

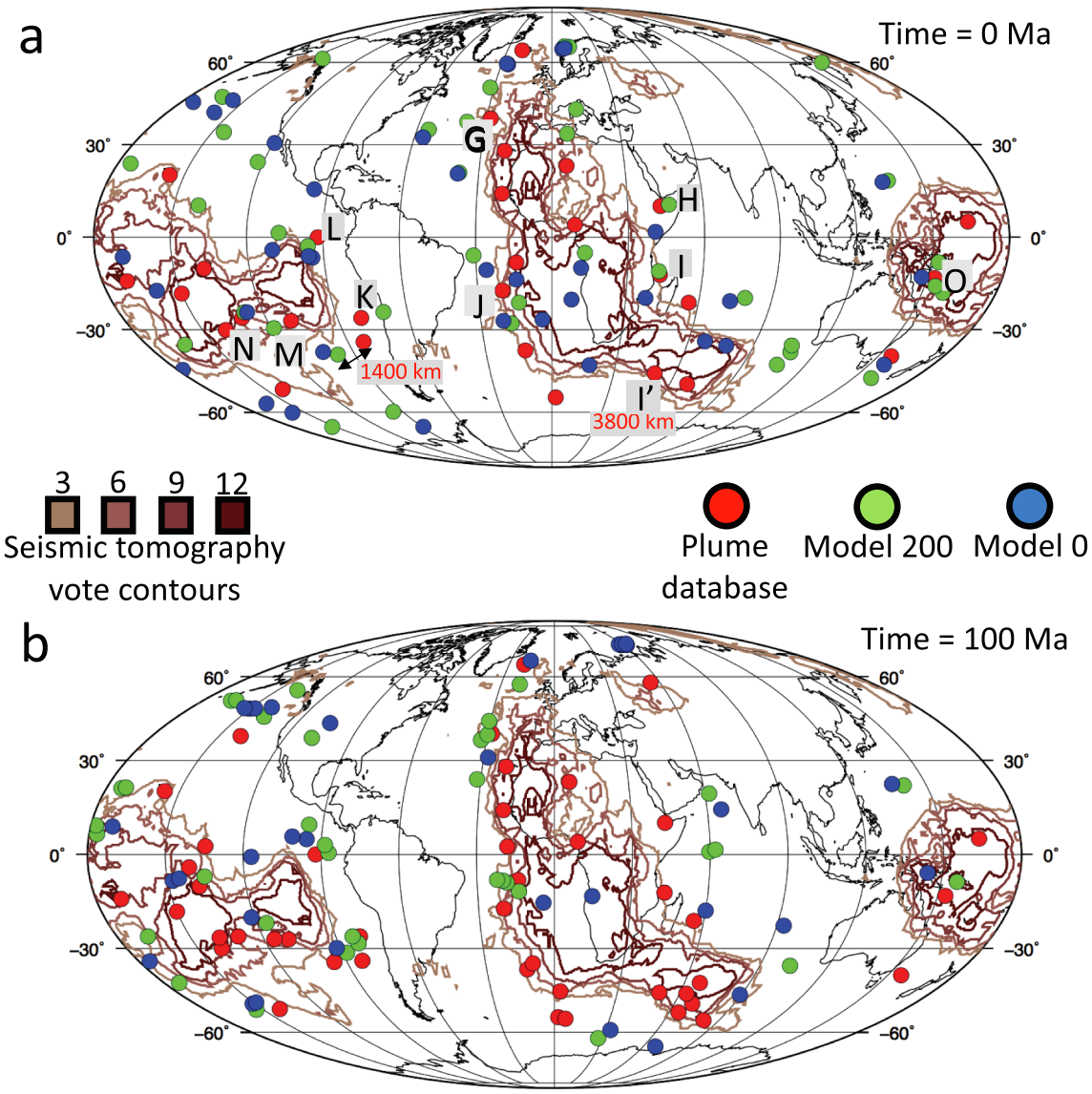

Fig. 9. A number of model upwellings form close to the edges of LLSVPs and reach close to the surface near observed present-day hotspots. a) Plume positions at 0 Ma for Model200 (green), Model0 (blue), and the approximate hotspot database (Steinberger, 2000; French and Romanowicz, 2015; Whittaker et al., 2015) (red) as given in Table 3. b) Plume positions at 100 Ma for the above models alongside a large igneous province database for 251 – 99 Ma (red) as given in Table 4 (Torsvik et al., 2006) (with present-day hotspot positions also given in red circles). Plume key: G: Azores; H: Afar; I: Comores; J: St Helena; K: San Felix; L: Galapagos; M: Easter; N: Pitcairn; O: Indonesia. Two markers are given to indicate plume distances: 1400 km is shown between the Juan Fernandez plume and the nearest Model200 output; and 3800 km between I and I' (representing the largest distance between a database plume and a Model200 output). (For interpretation of the references to colour in this figure legend, the reader is referred to the web version of this article.)

3.3. *Distance from database analysis*

To test how statistically relevant our results are, we look at the distance of each of our model plumes (at 700 km depth) from the nearest present-day hotspot in the database (assuming sub-vertical ascent of the plume in the upper mantle, Table 3). Fig. 10 shows the percentage of database hotspots as a function of their distance from the nearest plume in Model0 (no thermo-chemical pile), Model200 (200 km initial thickness), and Model300 (300 km initial thickness). A lower distance for the database plume percentage indicates that there is a better fit between modeled plume positions and the location of hotspots in the database (e.g., the model is performing well). For instance, Model300 shows that all of the model plumes fall within 4000 km of a database plume. However, less than 48 % of the database plumes fall within 1500 km of a Model300 plume. In comparison, Model0 and Model200 perform much better, with 51 % and 59 % of the database plumes, respectively, falling within 1500 km or less from a model plume.

Fig. 10 also shows 10,000 randomly generated sets of 39 plume positions (grey lines). The percentile distribution of these artificially generated points is given by the areas shaded in grey and shows what percentage of the random models falls within a specific distance. In the case of the lightest grey area, less than 15 % of the random models have smaller distances to the database plumes than shown. The profiles of Model0 and Model200 follows this 15 % line closely, indicating that these models perform better than 85 % of the randomly generated results.

Fig. 11 provides an overall summary of the results in Fig. 10, and highlights the spread of the 10,000 randomly generated models. Specifically, it shows the median distance of the database plumes from the model plumes. For instance, the median distance for Model200 is

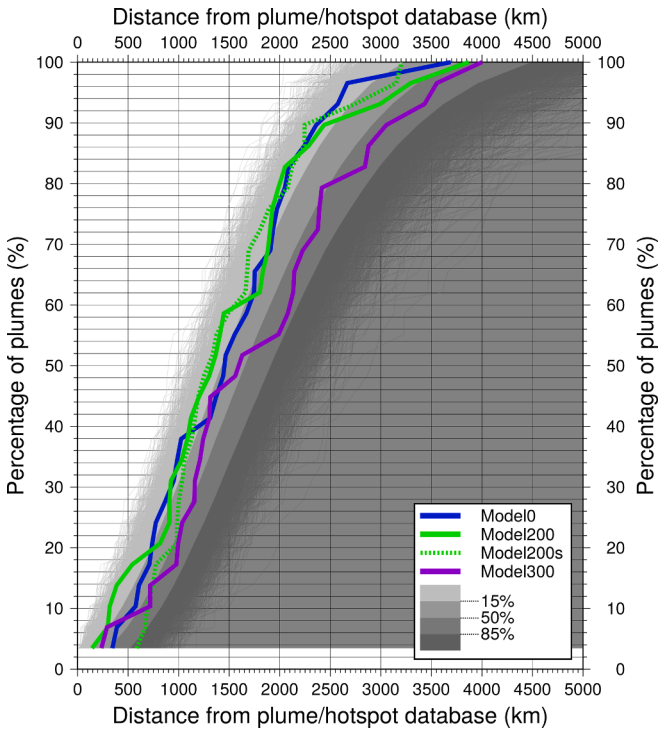

Fig. 10. Analysis of model plume positions at 0 Ma as a function of distance away from the nearest present-day hotspot (Table 3). For any distance given on the x-axis, the blue, green and purple lines show the percentage of model plumes that reach the surface closer to an observed present-day hotspot than this distance (for details on the analysis, see the Methods section). The purely thermal Model0 generates 37 plumes; Model200 (starting from a basal layer of dense material with 200 km thickness) features 39 plumes; and Model300 (with a 300-km basal layer) produces 32 plumes. Model200s utilizes 410 Myr of palaeo-subduction history using a modified reconstruction history (see Table 2) and produces 29 plumes. Grey lines show 10,000 sets of 39 artificially generated random plume positions. The shaded grey areas indicate the percentile distance distribution 15 %, 50 %, and 85 % of the 10,000 random models (see also Fig. 11). For most distances, Model0 and Model200 perform within the best 15 % of the random plume distributions (light grey). (For interpretation of the references to colour in this figure legend, the reader is referred to the web version of this article.)

approximately 1375 km (as shown in Fig. 10), which is nearly as low as the top 5 % of random models. Model0 produces a similar median at approximately 1475 km.

To further quantify this close relationship with Model200 and Model0 plumes, we present a plume comparison in Fig. 12. More than half of the Model0 plumes form within a radius of 900 km from the Model200 plumes (Fig. 12), indicating that the thermo-chemical pile may not be the driving force in plume positioning.

3.4. Shorter subduction history

One model featured in the results that hasn't been fully explained so far is Model200s, which has been generated to test the impact of a shortened realistic subduction history. Model200s applies a 410 Myr plate reconstruction that uses an extended version of Seton et al. (2012) (where the Seton et al. (2012) 250 Ma to 90 Ma surface velocities are used for our model 410 Ma to 250 Ma, then repeated from 250 Ma until present-day (Bower et al., 2013)). We apply this unrealistic velocity history to purposefully not represent past plate motions well. In applying these surface velocities, we can test the relative importance of supercontinent formation (e.g., 410 Ma to 250 Ma) in developing plume positions.

Fig. 10 indicates that Model200s performs as well as Model200 for the majority of database plumes. However, the surface velocities from the more recent global model of Matthews et al. (2016) that incorporate supercontinent formation do have an impact on the shape of the thermo-chemical piles in our models. Fig. 5 indicates that applying appropriate surface velocities for the final 250 Myr (e.g., Model200s) is not enough time to completely constrain the outline of the thermo-chemical pile beyond its general position. Although there is good agreement between the TCP and the Pacific LLSVP, the African thermo-chemical pile appears to be at a higher latitude when compared to a model that has undergone supercontinent formation and dispersal surface velocities (e.g., Model200).

3.5. High resolution

To test the impact of resolution on our model results, we also computed a higher-resolution convection simulation with the same setup as Model200. Compared to Model200, we increased the resolution by a factor of two, reduced the time step size by a factor of 2, and reduced the nonlinear solver tolerance from 10^{-3} to 10^{-5}. The results of this Model200hr are shown in Figs. 13-15. The position of the thermo-chemical piles on an equatorial slice are similar in both models but not equal between the models. The higher resolution model requires less stabilization for the advection equation, reducing the thickness of cold downwellings as shown in Fig. 13.

For the same reason, we also find that in the upper mantle, the upwelling plumes are thinner and not as hot in the higher resolution model. To generate a similar number of model plumes for the statistical analysis as in the other models, we define plumes as regions with an excess temperature of at least 200 K at 700 km depth (rather than 300 K as in Model200). This classification produces 29 Model200hr plumes in positions shown by the white circles in Fig. 14. The plume positions are not identical to the lower resolution model (Fig. 14a) and the thermo-chemical pile covers more of the core-mantle boundary than in Model200 (Fig. 14b). However, Fig. 15 does show that the results are robust with regards to the plume positioning consistently performing better than the random models.

4. Discussion

In this study, we compare present-day hotspot positions to models with and without thermo-chemical piles (Fig. 9a). We find that models both with and without these chemical heterogeneities can produce plumes close to present-day hotspots. This finding is in keeping with a number of previous studies that highlight that LLSVPs could be a relatively passive feature of mantle dynamics (as shown in Fig. 4), and that ancient subducted ocean plates, rather than chemical heterogeneity, are the dominant factor driving global mantle circulation (e.g., McNamara and Zhong, 2005; Bower et al., 2013; Davies et al., 2012, 2015; Davies and Davies, 2009; Hassan et al., 2015; Steinberger and Torsvik, 2012; Flament et al., 2022).

4.1. Geodynamic implications

The work presented here has wider implications for mantle dynamics. The proximity of ancient large igneous provinces (LIPs) to the edges of present-day LLSVPs has often been cited as a reason why deep mantle heterogeneities may be dynamically stable over 500 Myr timeframes (Torsvik et al., 2006, 2008). By analysing the upwelling locations for Model200 and Model0 during the Cretaceous (100 million years in the past), the position of plumes still often occurs near the margins of present-day LLSVPs (Fig. 9b). This is significant given that our thermo-chemical piles are not fixed over time (Figs. 3 and 4) or not even present at all (e.g., Model0). Consequently, LLSVPs do not need to be laterally fixed on supercontinent timescales (Torsvik et al., 2006, 2008) to produce appropriate plume positions in the present or

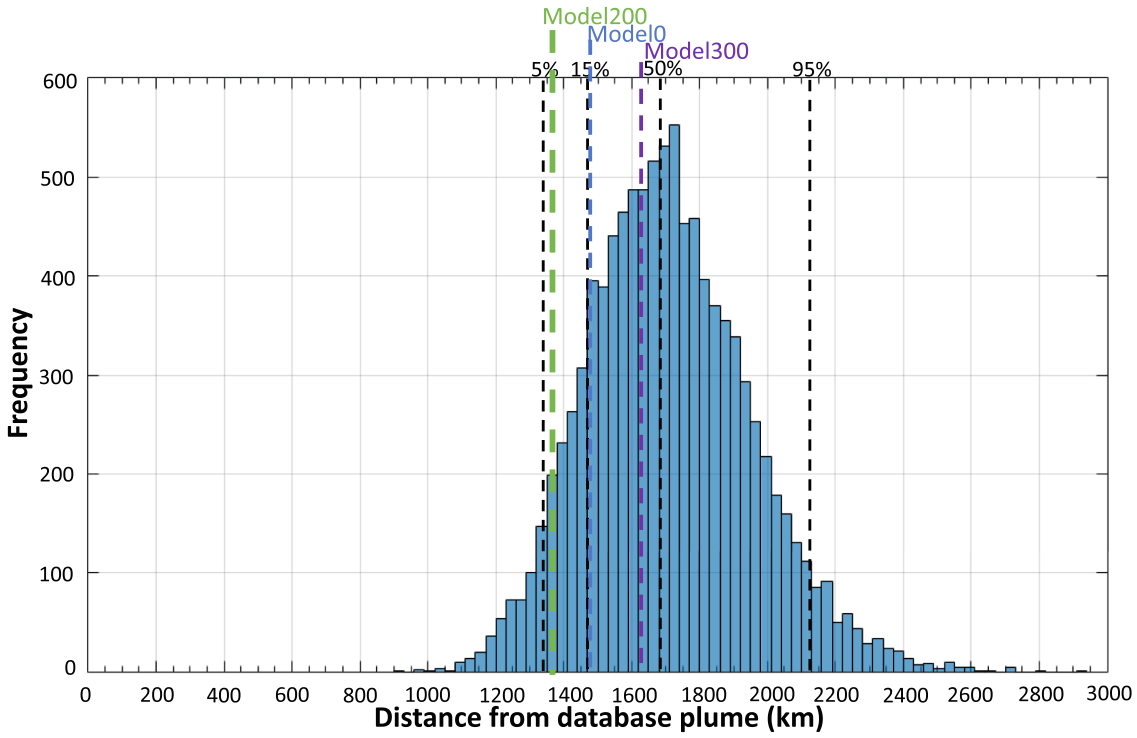

Fig. 11. Model200 performs better than around 95% of the 10,000 random models. Histogram showing the spread of median distances of the randomly generated plumes as compared to the database plumes. Annotated are the 5%, 15%, 50%, and 95% distributions of the random models, as well as the Model200, Model0, and Model300 results.

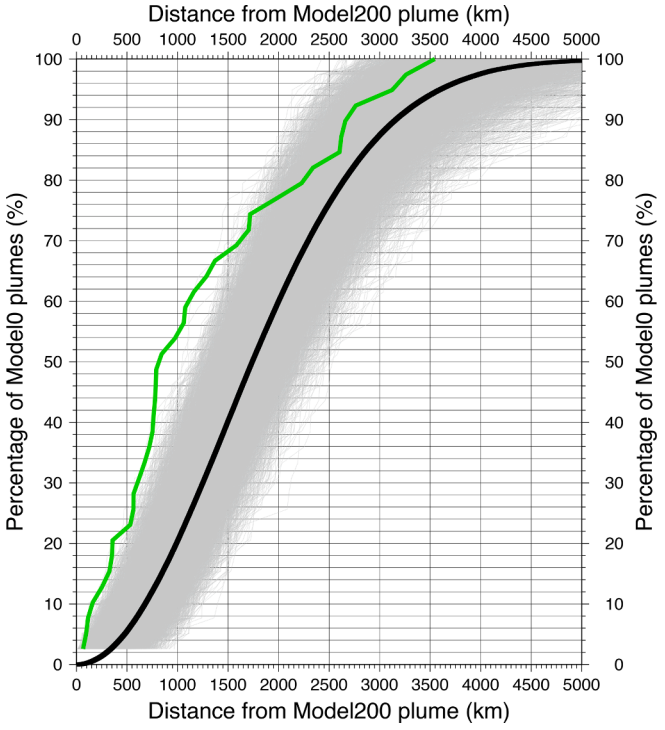

Fig. 12. Analysis of Model0 plume positions at 0 Ma as a function of distance away from nearest Model200 plume. Models have differing number of plumes (see main text). Model0 features no thermo-chemical pile (TCP) and Model200 has a 200 km initial TCP thickness. The black line is the accumulation of 10,000 sets of 39 random plume positions artificially generated (grey lines).

(potentially) in the past.

Instead, the relative stability of subduction zones over the last 200 million years may be the crucial factor for fixing the proximity of past plumes to present-day LLSVP margins. Our models indicate a decoupling of mantle timescales for plume positions (short scale) and LLSVP dynamics (longer scale), controlled by the plate motion history.

This point is highlighted by analysing the development of plumes and the positioning of LLSVPs beneath Africa and the Pacific in Model200s. By only running appropriate plate reconstruction history for the past 250 Ma (instead of 410 Ma in Model200), Model200s does not produce a thermo-chemical pile in the southern hemisphere under Africa (Fig. 5e). However, in analysis of the plume positions, Model200s performs as well as Model200 (Fig. 10).

Although we highlight that LLSVPs do not need to be spatially fixed over supercontinent timescales, our models do not, and cannot, rule out LLSVPs being either purely thermal anomalies (Model0), (meta)stable chemical piles of dense material (Model200), or a combination of the two (Model100) (Fig. 8). In contrast to our work, previous studies found that a thermo-chemical simulation, rather than a purely thermal model, is required to produce appropriate plume positions for present-day hotspots (Steinberger and Torsvik, 2012; Hassan et al., 2015; Li and Zhong, 2017). However, Davies et al. (2012) previously showed that observed lower mantle shear wave velocity anomalies do not require large-scale chemical piles to obtain appropriate LLSVP dynamics. Although Davies et al. (2012) did not conduct a formal plume analysis as given in our study, they did find that purely thermal LLSVPs (e.g., isochemical) could reconcile observed shear wave velocity anomalies and gradients. The work presented in our study highlights that purely thermal geodynamic models can not only produce seismological features of the deep mantle (e.g., Davies et al., 2012), but also reproduce mantle dynamics in the form of plume locations (Fig. 9a). This finding is also in keeping with the results of Hassan et al. (2015).

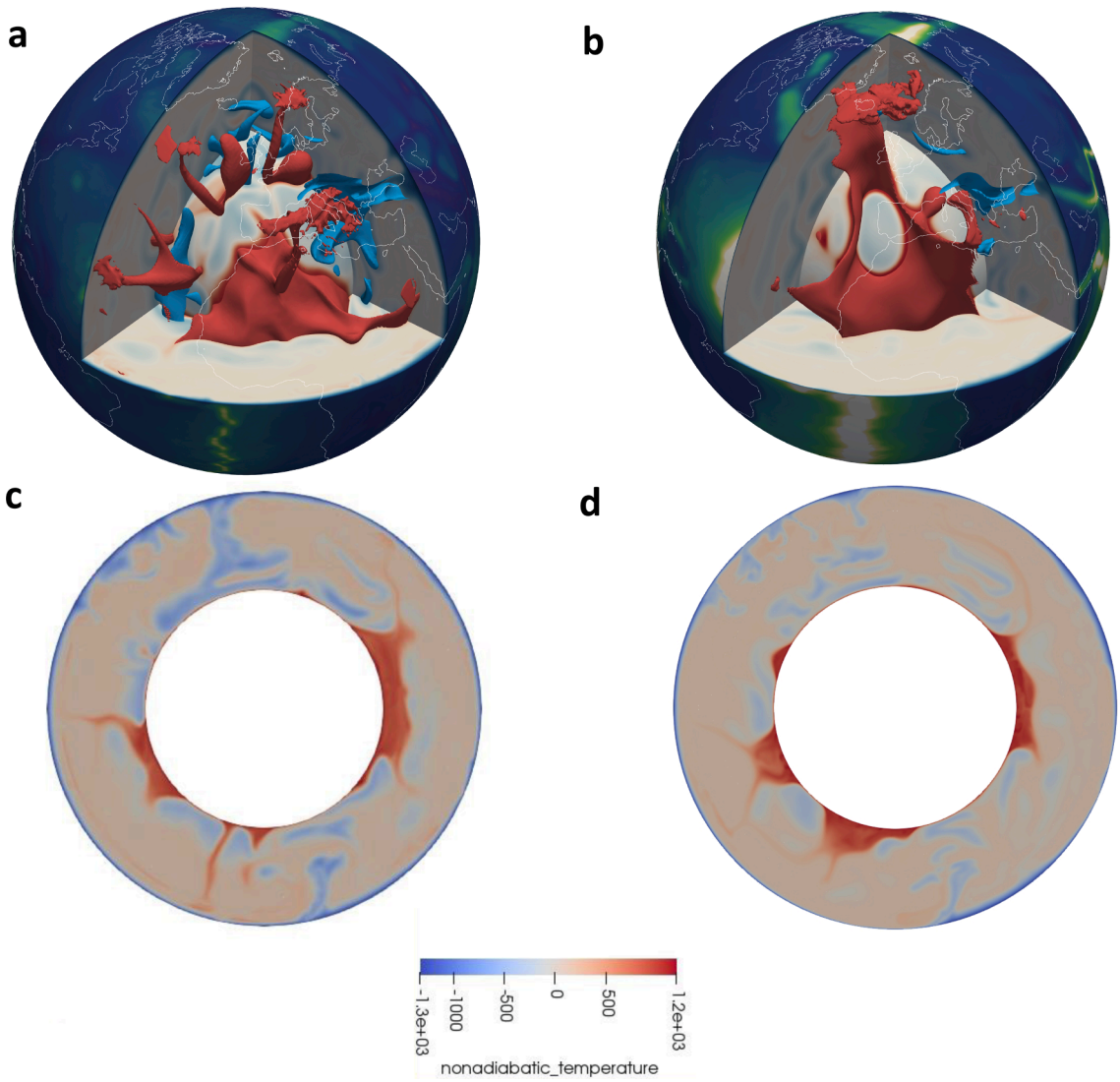

Fig. 13. Comparison between Model200 and Model200hr (a higher resolution simulation). Figure shows a view into the mantle beneath the northern Atlantic and Europe for Model200 (a) and Model200hr (b). Excess temperature anomaly contours are given for warm (300 K, red) and cold (−500 K, blue) regions. Excess temperature at the equator is given for Model200 (c) and Model200hr (d). (For interpretation of the references to colour in this figure legend, the reader is referred to the web version of this article.)

4.2. Future work

Although we present models with and without anomalous piles of material near the base of the mantle, we do not explore the potential impact of the density and geometry of the deep LLSVP material on our findings (and only present the end-member cases). Denser and less mobile piles of material could have a control on plume locations and plume generation, given their potential impact on the core–mantle heat flow. Furthermore, the impact of changing the initial condition of our numerical models (e.g. temperature profile) would also assist in placing our findings within the context of Earth's secular evolution. Currently, this extensive testing is out of the scope of this study, but our prescribed buoyancy number is within potential estimates for the deep mantle anomaly (Garnero et al., 2016).

Our work here implies that the decoupling of plume generation and large-scale mantle flow timescales makes it difficult to unravel the composition of LLSVPs from numerical models alone (Fig. 8). As a result, we posit that the key to understanding the seismic anomalies in the present-day deep mantle can only come from direct sampling, and we therefore encourage additional geochemical data and seismologic observations. However, there are still various aspects related to the numerical experiments and geological analyses that would be intriguing to explore further. In particular, future work on these models could incorporate longer plate reconstruction histories (e.g., 1 Gyr Merdith et al. (2021)) than our surface velocities going back to 410 Ma (e.g., Cao et al., 2021a,b; Flament et al., 2022).

Furthermore, in this study we imply that all hotspots can be related to deep-mantle plumes, which may not be the case. Future work would be to make progress in the debate on which present-day hotspots could be candidates for a deep mantle plume origin. In addition, future work here would benefit from more detailed comparison of our numerical simulations with available seismic and geochemical data (e.g., Davaille and Romanowicz, 2020; Hosseini et al., 2018).

However, the work presented here does only focus on plumes generated through a deep mantle source. As a result, future work would require analysis that takes into consideration plumes forming from an upper mantle source, either through plate tectonic collapse (e.g., Petersen et al., 2018) or through secondary and/or 'baby' plumes (e.g., Koptev et al., 2021; Cloetingh et al., 2022). Furthermore, in our study here we apply a 300 K excess temperature at a depth of 700 km for plume identification, but growing evidence for a hydrous mantle transition zone (e.g., Helffrich and Wood, 2001; Kuritani et al., 2011, 2019)

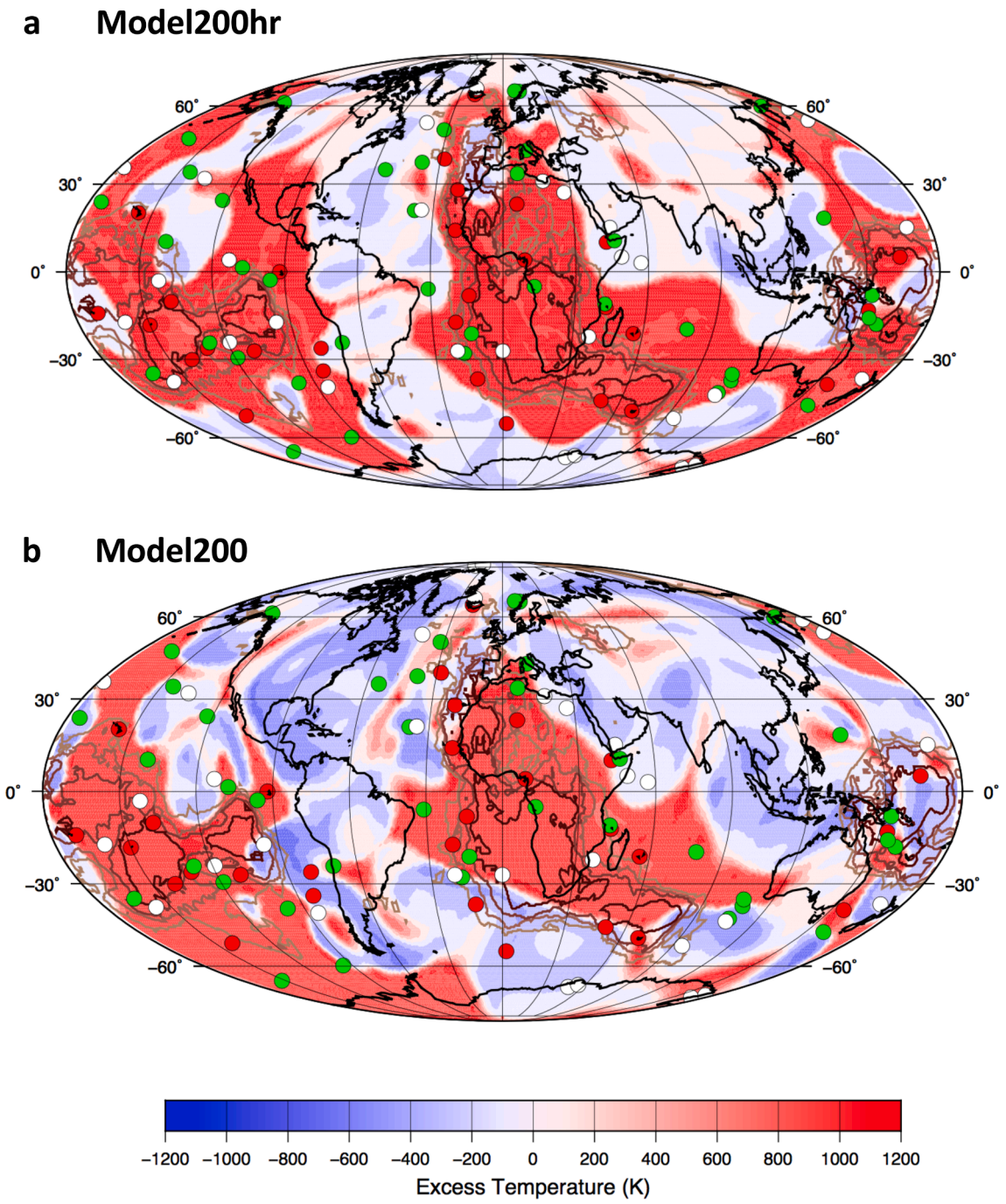

Fig. 14. Comparison between Model200 and Model200hr (a higher resolution simulation). The excess temperature at 2800 km depth for Model200hr is given in (a), with seismic tomography vote contours as Fig. 1. Green circles and white circles show Model200 and Model200hr plume positions, respectively. Red circles are of the approximate present-day plume database (Table 3). See Methods for Model200hr description. The excess temperature at 2800 km depth for Model200 is given in (b) for comparison. Circles as (a). (For interpretation of the references to colour in this figure legend, the reader is referred to the web version of this article.)

may reduce the need for such high temperatures for plume classification (Cloetingh et al., 2022). Future analysis may wish to test this criteria for plume identification.

4.3. Uncertainty discussion

Our work here is a one of a number of numerical modelling papers on a similar topic: applying plate reconstruction histories to develop mantle dynamics. Given the increase in computational power available in comparison to a decade ago, it may be appropriate to discuss as a community the key parameters needed in these sorts of studies. What are the fundamental aspects for this area of geoscience?

For instance, we should discuss a standard for determining if a model 'fits' available data and establish what constitutes where a model plume overlaps with an observed plume or ancient large igneous province position. As such, we could discuss a community standard for deviation from this distance (e.g., 10 km, 100 km or 1,000 km?). Our work here quantifies the plume positions to a database but we acknowledge that this is not an easy task for a reader to immediately grasp. We think it would be worthwhile to develop a community standard that we can

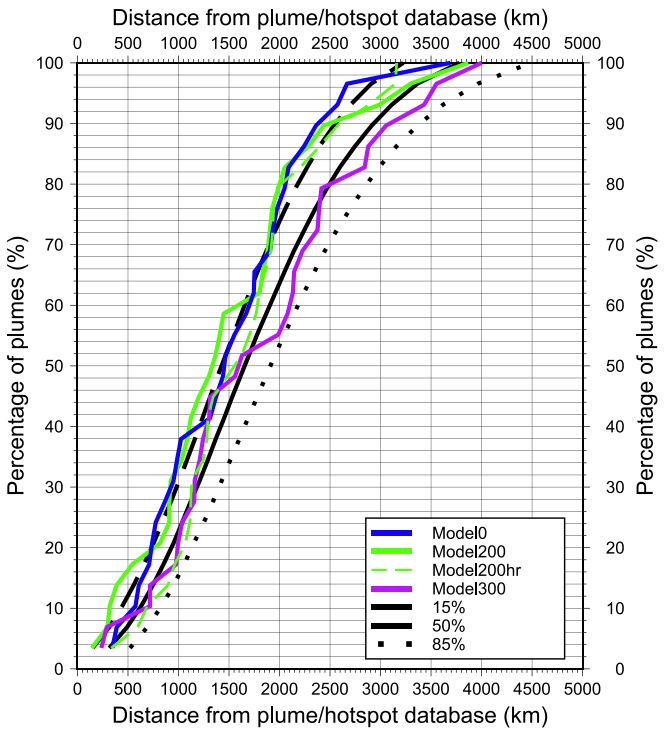

Fig. 15. Analysis of model plume positions at 0 Ma as a function of distance away from nearest present-day plume (Table 3). This image is as Fig. 10 (see caption for details) but with the addition of a high resolution Model200 (Model200hr). See Methods for description of high resolution model.

apply to create statistically relevant analysis of these large global models that also allows for an easy comparison between the quality of fit in different studies (e.g., Austermann et al., 2014; Hassan et al., 2015; Davies et al., 2015).

A further area of discussion would be the need to test initial conditions for these large models to understand the robustness of the results, alongside the potential for a specific time range for applying plate reconstruction histories as surface velocities (e.g., 410 Ma or 1 Ga). In regard to the initial condition of such geodynamic explorations, mantle convection simulations can be run from an undisturbed mantle case (as in this study), or a specific mantle configuration (e.g., Hassan et al., 2015; Heron and Lowman, 2010), or after a defined spin-up phase where the model equilibrates into a steady state (e.g., Yoshida et al., 1999; Heron and Lowman, 2011). These initial mantle conditions could induce their own thermal instabilities within the system that may continue and evolve throughout the model simulation, as outlined in Weller and Lenardic (2012). However, Colli et al. (2015) highlighted the longevity of the impact of an initial condition in models that feature prescribed surface velocities may be around 300 Myr. In our work presented here, we analyse mantle dynamics a significant time after the initial condition (>300 Myr), with a particular focus on present-day (e.g., 410 Myr after the model simulation begins), to attempt to negate any such impact of implementing an undisturbed mantle as an initial condition.

For models simulating mantle history from the Devonian to the present day (as in this study), there are also assumptions on the initial location and geometries of modelled LLSVPs that could be pertinent to the development of the model. Here we start from an idealized state that our modelled LLSVPs are a uniform layer of 0–300 km thickness around the core-mantle boundary (Table 2). A difficulty here is the uncertainty involved in LLSVP extent in the Devonian mantle. A better understanding of the impact of the initial location and extent of thermo-chemical piles in such models would be an area of discussion (e.g., Zhong and Rudolph, 2015; Bower et al., 2013; Gassmöller, 2020), alongside the smaller scale dynamics of a mantle convection initial condition (e.g., downwellings and upwellings).

For global plate reconstructions, a number of available models apply a method of tracing large igneous province locations back to the edge of LLSVPs (e.g., Domeier and Torsvik, 2014). As a result, there is a potential feedback loop between downwellings controlling thermo-chemical pile positions and resultant plume locations. An exploration into the impact of alternative absolute reference frames would be welcome as would, further work on coupling self-generating plate tectonic models (e.g., Tackley, 2000; Rolf and Tackley, 2011; Langemeyer et al., 2022) with the top-down driven simulations (as shown here in the study). By specifying the top-down velocity conditions through plate reconstruction histories driving the thermal evolution of our models, we cannot unravel the overall control on mantle dynamics.

As highlighted here, there may be a need to specify resolution limits for such large models. Similarly, a comparison of Rayleigh numbers across the different models would also be important (e.g., Heron and Lowman, 2014). The paper here offers insights into our numerical models of global mantle convection in relation to deep mantle dynamics, but we also wish to understand the uncertainty generated from such simulations, and highlight the need for 'industry standards' on this type of work.

5. Conclusions

In this study, we prescribe a plate reconstruction history as a time-dependent surface condition to evolve the mantle, and compare our numerical simulations with present-day hotspots and seismic tomography. The numerical models presented here show that subduction alone can produce the location and timing of some present-day hotspots (which we interpret as manifestations of deep mantle plumes).

Our experiment changes the thickness of a thermo-chemical dense layer at the base of mantle and compares the impact on the plume positions as this layer evolves. A significant result is that we are able to produce similar plume positions for models where the deep mantle layer is chemically distinct or purely thermal (Fig. 9).

For some of the models presented here, the meta-stability of these deep mantle structures can be cogent with observed mantle dynamics (Fig. 6) and we suggest that the deep mantle may evolve as significantly as our tectonic surface (Figs. 3 and 4).

CRediT authorship contribution statement

Philip J. Heron: Writing – review & editing, Writing – original draft, Visualization, Validation, Software, Resources, Project administration, Methodology, Investigation, Funding acquisition, Formal analysis, Data curation, Conceptualization. **Juliane Dannberg:** Writing – review & editing, Writing – original draft, Methodology, Investigation, Data curation, Conceptualization. **Rene Gassmöller:** Writing – review & editing, Visualization, Methodology. **Grace E. Shephard:** Writing – review & editing, Writing – original draft, Visualization, Methodology, Investigation. **Jeroen van Hunen:** Writing – review & editing, Writing – original draft, Resources, Methodology. **Russell N. Pysklywec:** Writing – review & editing, Writing – original draft, Resources, Methodology.

Declaration of competing interest

The authors declare that they have no known competing financial interests or personal relationships that could have appeared to influence the work reported in this paper.

Acknowledgments

We would like to thank the Editor, Daniel Pastor-Galán, and an anonymous reviewer for their thoughtful comments on this paper. A special thank you to Prof Santosh for considering this work.

Financial support

This publication is part of a project that has received funding from the European Union's Horizon 2020 research and innovation program under the Marie Skłodowska-Curie Grant Agreement 749664 (P. J. Heron). This research was enabled in part by support provided by Compute Ontario (computeontario.ca) and the Digital Research Alliance of Canada (alliancecan.ca) for allocations to PJH and RP. We also acknowledge support from a Natural Sciences and Engineering Research Council of Canada Discovery Grants for PJH and RP. JD gratefully acknowledges the support of the Deep Carbon Observatory. GES. acknowledges support from the Research Council of Norway through its Centers of Excellence funding scheme, Project Number 332523, and through its Young Research Talent scheme for 'POLARIS – Evolution of the Arctic in Deep Time', Project Number 326238. JD and RG were supported by the NSF grants EAR-2054605 and EAR-1925677. JvH. acknowledges nancial support from NERC (NE/M000281/1). The authors acknowledge the Texas Advanced Computing Center (TACC, http://www.tacc.utexas.edu) at The University of Texas at Austin for providing high-performance computing resources that have contributed to the research results reported within this paper. We thank the Computational Infrastructure for Geodynamics (geodynamics.org), which is funded by the National Science Foundation under awards EAR-2149126, EAR-0949446, and EAR-1550901, for supporting the development of ASPECT.

References

Allègre, C.J., 1982. Chemical geodynamics. Tectonophysics 81, 109–132. https://doi.org/10.1016/0040-1951(82)90125-1 geo- physics nal symposium.

Allègre, C.J., Turcotte, D.L., 1986. Implications of a two-component marble-cake mantle. Nature 323, 123–127. https://doi.org/10.1038/323123a0.

Austermann, J., Kaye, B.T., Mitrovica, J.X., Huybers, P., 2014. A statistical analysis of the correlation between large igneous provinces and lower mantle seismic structure. Geophys. J. Int. 197, 1–9. https://doi.org/10.1093/gji/ggt500.

Bower, D.J., Gurnis, M., Seton, M., 2013. Lower mantle structure from paleogeographically constrained dynamic Earth models. Geochem. Geophys. Geosyst. 14, 44–63. https://doi.org/10.1029/2012gc004267.

Bull, A.L., Domeier, M., Torsvik, T.H., 2014. The effect of plate motion history on the longevity of deep mantle heterogeneities. Earth Planet. Sci. Lett. 401, 172–182. https://doi.org/10.1016/j.epsl.2014.06.008.

Burke, K., 2011. Plate Tectonics, the Wilson Cycle, and Mantle Plumes: Geodynamics from the Top. Annu. Rev. Earth Planet. Sci. 39, 1–29. https://doi.org/10.1146/annurev-earth-040809-152521.

Burov, E., Cloetingh, S., 2010. Plume-like upper mantle instabilities drive subduction initiation. Geophys. Res. Lett. 37. https://doi.org/10.1029/2009GL041535.

Cao, X., Flament, N., Bodur, Ö. F., and Müller, R. D.: The evolution of basal mantle structure in response to supercontinent aggregation and dispersal, Scienti c Reports, 11, 22 967, 10.1038/s41598-021-02359-z, 2021a.

Cao, X., Flament, N., and Müller, R. D.: Coupled Evolution of Plate Tectonics and Basal Mantle Structure, Geochemistry, Geophysics, Geosystems, 22, e2020GC009 244, 10.1029/2020GC009244, e2020GC009244 2020GC009244, 2021b.

Carlson, R.W., 1994. Mechanisms of Earth differentiation: consequences for the chemical structure of the mantle. Rev. Geophys. 32, 337. https://doi.org/10.1029/94rg01874.

Cloetingh, S., Koptev, A., Kovács, I., Gerya, T., Beniest, A., Willingshofer, E., Ehlers, T. A., Andric´-Tomaševic´, N., Bot- syun, S., Eizenhöfer, P. R., François, T., and Beekman, F.: Plume-Induced Sinking of Intracontinental Lithospheric Man- tle: An Overlooked Mechanism of Subduction Initiation?, Geochemistry, Geophysics, Geosystems, 22, e2020GC009482, 10.1029/2020GC009482, e2020GC009482 2020GC009482, 2021.

Cloetingh, S., Koptev, A., Lavecchia, A., Kovács, I. J., and Beekman, F.: Fingerprinting secondary mantle plumes, Earth and Planetary Science Letters, 597, 117 819, 10.1016/j.epsl.2022.117819, 2022.

Colli, L., Bunge, H.-P., Schuberth, B., 2015. On retrodictions of global mantle ow with assimilated surface velocities. Geophys. Res. Lett. 42, 8341–8348. https://doi.org/10.1002/2015GL066001.

Connolly, J.A.D., 2009. The geodynamic equation of state: What and how. Geochem. Geophys. Geosyst. 10. https://doi.org/10.1029/2009gc002540 n/a–n/a.

Cottaar, S., Lekic, V., 2016. Morphology of seismically slow lower-mantle structures. Geophys. J. Int. 207, 1122–1136. https://doi.org/10.1093/gji/ggw324.

Dannberg, J., Gassmoeller, R., Thallner, D., LaCombe, F., and Sprain, C.: Changes in core-mantle boundary heat ux patterns throughout the supercontinent cycle, 2023.

Dannberg, J., Gassmöller, R., 2018. Chemical trends in ocean islands explained by plume–slab interaction. Proc. Natl. Acad. Sci. 115, 4351–4356. https://doi.org/10.1073/pnas.1714125115.

Davaille, A. and Romanowicz, B.: De ating the LLSVPs: Bundles of Mantle Thermochemical Plumes Rather Than Thick Stagnant "Piles", Tectonics, 39, e2020TC006 265, 10.1029/2020TC006265, e2020TC006265 10.1029/2020TC006265, 2020.

Davies, D., Davies, J., 2009. Thermally-driven mantle plumes reconcile multiple hot-spot observations. Earth Planet. Sci. Lett. 278, 50–54. https://doi.org/10.1016/j.epsl.2008.11.027.

Davies, D.R., Goes, S., Davies, J., Schuberth, B., Bunge, H.-P., Ritsema, J., 2012. Reconciling dynamic and seismic models of Earth's lower mantle: The dominant role of thermal heterogeneity. Earth Planet. Sci. Lett. 353–354, 253–269. https://doi.org/10.1016/j.epsl.2012.08.016.

Davies, D., Goes, S., Sambridge, M., 2015. On the relationship between volcanic hotspot locations, the reconstructed erup- tion sites of large igneous provinces and deep mantle seismic structure. Earth Planet. Sci. Lett. 411, 121–130. https://doi.org/10.1016/j.epsl.2014.11.052.

Deschamps, F., Trampert, J., 2003. Mantle tomography and its relation to temperature and composition. Phys. Earth Planet. In. 140, 277–291. https://doi.org/10.1016/j.pepi.2003.09.004.

Deschamps, F., Cobden, L., Tackley, P.J., 2012. The primitive nature of large low shear-wave velocity provinces. Earth Planet. Sci. Lett. 349–350, 198–208. https://doi.org/10.1016/j.epsl.2012.07.012.

Domeier, M., Torsvik, T.H., 2014. Plate tectonics in the late Paleozoic. Geosci. Front. 5, 303–350. https://doi.org/10.1016/j.gsf.2014.01.002.

Farnetani, C.G., Hofmann, A.W., Class, C., 2012. How double volcanic chains sample geochemical anomalies from the lowermost mantle. Earth Planet. Sci. Lett. 359–360, 240–247. https://doi.org/10.1016/j.epsl.2012.09.057.

Flament, N., Bodur, Ö.F., Williams, S.E., Merdith, A.S., 2022. Assembly of the basal mantle structure beneath Africa. Nature 603, 846–851. https://doi.org/10.1038/s41586-022-04538-y.

Flament, N., Williams, S., Müller, R. D., Gurnis, M., and Bower, D. J.: Origin and evolution of the deep thermochemical structure beneath Eurasia, Nature Communications, 8, 14 164, 10.1038/ncomms14164, 2017.

French, S.W., Romanowicz, B.A., 2014. Whole-mantle radially anisotropic shear velocity structure from spectral-element waveform tomography. Geophys. J. Int. 199, 1303–1327. https://doi.org/10.1093/gji/ggu334.

French, S.W., Romanowicz, B., 2015. Broad plumes rooted at the base of the Earth's mantle beneath major hotspots. Nature 525, 95–99. https://doi.org/10.1038/nature14876.

Garnero, E.J., McNamara, A.K., Shim, S.-H., 2016. Continent-sized anomalous zones with low seismic velocity at the base of Earth's mantle. Nat. Geosci. 9, 481–489. https://doi.org/10.1038/ngeo2733.

Gassmöller, R.: The interaction of subducted slabs and plume generation zones in geodynamic models, Ph.D. thesis, University of Potsdam, 10.5281/zenodo.3516433, 2020.

Gonnermann, H.M., Mukhopadhyay, S., 2007. Non-equilibrium degassing and a primordial source for helium in ocean-island volcanism. Nature 449, 1037–1040. https://doi.org/10.1038/nature06240.

Gonnermann, H.M., Mukhopadhyay, S., 2009. Preserving noble gases in a convecting mantle. Nature 459, 560–563. https://doi.org/10.1038/nature08018.

Hassan, R., Müller, R.D., Gurnis, M., Williams, S.E., Flament, N., 2016. A rapid burst in hotspot motion through the interaction of tectonics and deep mantle ow. Nature 533, 239–242. https://doi.org/10.1038/nature17422.

Hassan, R., Flament, N., Gurnis, M., Bower, D. J., and Müller, D.: Provenance of plumes in global convection models, Geochemistry, Geophysics, Geosystems, 16, 1465–1489, 10.1002/2015gc005751, 2015.

Heister, T., Dannberg, J., Gassmöller, R., Bangerth, W., 2017. High Accuracy Mantle Convection Simulation through Modern Numerical Methods. II: Realistic Models and Problems. Geophys. J. Int. 210, 833–851. https://doi.org/10.1093/gji/ggx195.

Helffrich, G.R., Wood, B.J., 2001. The Earth's mantle. Nature 412, 501–507. https://doi.org/10.1038/35087500.

Heron, P. J., Gün, E., Shephard, G. E., Dannberg, J., Gassmöller, R., Martin, E., Sharif, A., Pysklywec, R. N., Nance, R. D., and Murphy, J. B.: The role of subduction in the formation of Pangaean oceanic large igneous provinces, Geological Society, London, Special Publications, 542, SP542–2023–12, 10.1144/SP542-2023-12, 2024.

Heron, P.J., Lowman, J.P., 2010. Thermal response of the mantle following the formation of a "super-plate". Geophys. Res. Lett. 37. https://doi.org/10.1029/2010gl045136 n/a–n/a.

Heron, P.J., Lowman, J.P., 2011. The effects of supercontinent size and thermal insulation on the formation of mantle plumes. Tectonophysics 510, 28–38. https://doi.org/10.1016/j.tecto.2011.07.002.

Heron, P.J., Lowman, J.P., 2014. The impact of Rayleigh number on assessing the signi cance of supercontinent insulation. J. Geophys. Res. Solid Earth 119, 711–733. https://doi.org/10.1002/2013jb010484.

Heron, P.J., Murphy, J.B., Nance, R.D., Pysklywec, R.N., 2021. Pannotia's mantle signature: the quest for supercontinent identi cation. Geol. Soc. Lond. Spec. Publ. 503, 41–61. https://doi.org/10.1144/SP503-2020-7.

Heron, P. J.: Mantle plumes and mantle dynamics in the Wilson cycle, Geological Society, London, Special Publications, p. SP470.18, 10.1144/sp470.18, 2018.

Heyn, B.H., Conrad, C.P., Trønnes, R.G., 2018. Stabilizing effect of compositional viscosity contrasts on thermochemical piles. Geophys. Res. Lett. 45, 7523–7532. https://doi.org/10.1029/2018GL078799.

Heyn, B. H., Conrad, C. P., and Trønnes, R. G.: How Thermochemical Piles Can (Periodically) Generate Plumes at Their Edges, Journal of Geophysical Research: Solid Earth, 125, e2019JB018 726, 10.1029/2019JB018726, e2019JB018726 10.1029/2019JB018726, 2020.

Hosseini, K., Matthews, K.J., Sigloch, K., Shephard, G.E., Domeier, M., Tsekhmistrenko, M., 2018. SubMachine: Web-Based Tools for Exploring Seismic Tomography and Other Models of Earth's Deep Interior. Geochem. Geophys. Geosyst. 19, 1464–1483. https://doi.org/10.1029/2018gc007431.

Ishii, M., 1999. Normal-mode and free-air gravity constraints on lateral variations in velocity and density of Earth's Mantle. Science 285, 1231–1236. https://doi.org/10.1126/science.285.5431.1231.

Jackson, M.G., Hart, S.R., Konter, J.G., Kurz, M.D., Blusztajn, J., Farley, K.A., 2014. Helium and lead isotopes reveal the geochemical geometry of the Samoan plume. Nature 514, 355–358. https://doi.org/10.1038/nature13794.

Karato, S.-i. and Karki, B. B.: Origin of lateral variation of seismic wave velocities and density in the deep mantle, Journal of Geophysical Research: Solid Earth, 106, 21 771–21 783, 10.1029/2001JB000214, 2001.

Koelemeijer, P., Deuss, A., and Ritsema, J.: Density structure of Earth's lowermost mantle from Stoneley mode splitting observations, Nature Communications, 8, 15 241, 10.1038/ncomms15241, 2017.

Koelemeijer, P.J., Deuss, A., Trampert, J., 2012. Normal mode sensitivity to Earth's D'' layer and topography on the core-mantle boundary: what we can and cannot see. Geophys. J. Int. 190, 553–568. https://doi.org/10.1111/j.1365-246x.2012.05499.x.

Koptev, A., Cloetingh, S., Ehlers, T.A., 2021. Longevity of small-scale ('baby') plumes and their role in lithospheric break-up. Geophys. J. Int. 227, 439–471. https://doi.org/10.1093/gji/ggab223.

Kronbichler, M., Heister, T., Bangerth, W., 2012. High Accuracy Mantle Convection Simulation through Modern Numerical Methods. Geophys. J. Int. 191, 12–29. https://doi.org/10.1111/j.1365-246X.2012.05609.x.

Kuritani, T., Ohtani, E., Kimura, J.-I., 2011. Intensive hydration of the mantle transition zone beneath China caused by ancient slab stagnation. Nat. Geosci. 4, 713–716. https://doi.org/10.1038/ngeo1250.

Kuritani, T., Xia, Q.-K., Kimura, J.-I., Liu, J., Shimizu, K., Ushikubo, T., Zhao, D., Nakagawa, M., Yoshimura, S., 2019. Buoyant hydrous mantle plume from the mantle transition zone. Scienti c Reports 9, 6549. https://doi.org/10.1038/s41598-019-43103-y.

Langemeyer, S.M., Lowman, J.P., Tackley, P.J., 2022. Contrasts in 2-D and 3-D system behaviour in the modelling of composition- ally originating LLSVPs and a mantle featuring dynamically obtained plates. Geophys. J. Int. 230, 1751–1774. https://doi.org/10.1093/gji/ggac143.

Lau, H. C. P., Mitrovica, J. X., Davis, J. L., Tromp, J., Yang, H.-Y., and Al-Attar, D.: Tidal tomography constrains Earth's deep-mantle buoyancy, Nature, 551, 321 EP –, 10.1038/nature24452, 2017.

Li, Z., Bogdanova, S., Collins, A., Davidson, A., Waele, B.D., Ernst, R., Fitzsimons, I., Fuck, R., Gladkochub, D., Jacobs, J., Karlstrom, K., Lu, S., Natapov, L., Pease, V., Pisarevsky, S., Thrane, K., Vernikovsky, V., 2008. Assembly, con guration, and break-up history of Rodinia: A synthesis. Precambrian Research 160, 179–210. https://doi.org/10.1016/j.precamres.2007.04.021 testing the Rodinia Hypothesis: Records in its Building Blocks.

Li, Z.-X., Zhong, S., 2009. Supercontinent–superplume coupling, true polar wander and plume mobility: Plate dominance in whole-mantle tectonics. Phys. Earth Planet. In. 176, 143–156. https://doi.org/10.1016/j.pepi.2009.05.004.

Li, M., Zhong, S., 2017. The source location of mantle plumes from 3D spherical models of mantle convection. Earth Planet. Sci. Lett. 478, 47–57. https://doi.org/10.1016/j.epsl.2017.08.033.

Masters, G., Gubbins, D., 2003. On the resolution of density within the Earth. Phys. Earth Planet. In. 140, 159–167. https://doi.org/10.1016/j.pepi.2003.07.008.

Matthews, K.J., Maloney, K.T., Zahirovic, S., Williams, S.E., Seton, M., Müller, R.D., 2016. Global plate boundary evolution and kinematics since the late Paleozoic. Global Planet. Change 146, 226–250. https://doi.org/10.1016/j.gloplacha.2016.10.002.

McNamara, A.K., Zhong, S., 2005. Thermochemical structures beneath Africa and the Paci c Ocean. Nature 437, 1136–1139. https://doi.org/10.1038/nature04066.

Merdith, A. S., Williams, S. E., Collins, A. S., Tetley, M. G., Mulder, J. A., Blades, M. L., Young, A., Armistead, S. E., Cannon, J., Zahirovic, S., and MÃŒller, R. D.: Extending full-plate tectonic models into deep time: Linking the Neoproterozoic and the Phanerozoic, Earth-Science Reviews, 214, 103 477, 10.1016/j.earscirev.2020.103477, 2021.

Müller, R.D., Seton, M., Zahirovic, S., Williams, S.E., Matthews, K.J., Wright, N.M., Shephard, G.E., Maloney, K.T., Barnett-Moore, N., Hosseinpour, M., Bower, D.J., Cannon, J., 2016. Ocean Basin Evolution and Global-Scale Plate Reorganization Events Since Pangea Breakup. Annu. Rev. Earth Planet. Sci. 44, 107–138. https://doi.org/10.1146/annurev-earth-060115-012211.

Nakagawa, T., Tackley, P. J., Deschamps, F., and Connolly, J. A. D.: Incorporating self-consistently calculated mineral physics into thermo- chemical mantle convection simulations in a 3-D spherical shell and its in uence on seismic anomalies in Earth's mantle, Geochemistry, Geophysics, Geosystems, 10, n/a–n/a, 10.1029/2008gc002280, 2009.

Ni, S., Tan, E., Gurnis, M., Helmberger, D., 2002. Sharp Sides to the African Superplume. Science 296, 1850–1852. https://doi.org/10.1126/science.1070698.

Nomura, R., Hirose, K., Uesugi, K., Ohishi, Y., Tsuchiyama, A., Miyake, A., Ueno, Y., 2014. Low Core-Mantle Boundary Temperature Inferred from the Solidus of Pyrolite. Science 343, 522–525. https://doi.org/10.1126/science.1248186.

Petersen, K. D., Schiffer, C., and Nagel, T.: LIP formation and protracted lower mantle upwelling induced by rifting and delamination, Scienti c Reports, 8, 16 578, 10.1038/s41598-018-34194-0, 2018.

Robson, A., Lau, H.C.P., Koelemeijer, P., Romanowicz, B., 2021. An analysis of core-mantle boundary Stoneley mode sensitivity and sources of uncertainty. Geophys. J. Int. 228, 1962–1974. https://doi.org/10.1093/gji/ggab448.

Rolf, T., Tackley, P.J., 2011. Focussing of stress by continents in 3D spherical mantle convection with self-consistent plate tectonics. Geophys- Ical Research Letters 38. https://doi.org/10.1029/2011GL048677.

Santosh, M., Maruyama, S., Yamamoto, S., 2009. The making and breaking of supercontinents: Some speculations based on superplumes, super downwelling and the role of tectosphere. Gondwana Research 15, 324–341. https://doi.org/10.1016/j.gr.2008.11.004, special Issue: Supercontinent Dynamics.

Santosh, M.: A synopsis of recent conceptual models on supercontinent tectonics in relation to mantle dynamics, life evolution and surface environment, Journal of Geodynamics, 50, 116–133, 10.1016/j.jog.2010.04.002, supercontinents and Crustal Evolution, 2010.

Schubert, G., Masters, G., Olson, P., Tackley, P., 2004. Superplumes or plume clusters? Phys. Earth Planet. In. 146, 147–162. https://doi.org/10.1016/j.pepi.2003.09.025.

Seton, M., Müller, R., Zahirovic, S., Gaina, C., Torsvik, T., Shephard, G., Talsma, A., Gurnis, M., Turner, M., Maus, S., Chandler, M., 2012. Global continental and ocean basin reconstructions since 200Ma. Earth Sci. Rev. 113, 212–270. https://doi.org/10.1016/j.earscirev.2012.03.002.

Shephard, G.E., Matthews, K.J., Hosseini, K., Domeier, M., 2017. On the consistency of seismically imaged lower mantle slabs. Scienti c Reports 7. https://doi.org/10.1038/s41598-017-11039-w.

Simmons, N.A., Forte, A.M., Boschi, L., Grand, S.P., 2010. GyPSuM: A joint tomographic model of mantle density and seismic wave speeds. J. Geophys. Res. 115. https://doi.org/10.1029/2010jb007631.

Steinberger, B., Calderwood, A.R., 2006. Models of large-scale viscous ow in the Earth's mantle with constraints from mineral physics and surface observations. Geophys. J. Int. 167, 1461–1481. https://doi.org/10.1111/j.1365-246x.2006.03131.x.

Steinberger, B., Torsvik, T.H., 2012. A geodynamic model of plumes from the margins of Large Low Shear Velocity Provinces. Geochem. Geophys. Geosyst. 13. https://doi.org/10.1029/2011gc003808 n/a–n/a.

Steinberger, B.: Plumes in a convecting mantle: Models and observations for individual hotspots, Journal of Geophysical Research: Solid Earth, 105, 11 127–11 152, 10.1029/1999jb900398, 2000.

Stixrude, L., Lithgow-Bertelloni, C., 2011. Thermodynamics of mantle minerals – II. Phase Equilibria. Geophys. J. Int. 184, 1180–1213. https://doi.org/10.1111/j.1365-246x.2010.04890.x.

Su, W. and Dziewonski, A. M.: Simultaneous inversion for 3-D variations in shear and bulk velocity in the mantle, Physics of the Earth and Planetary Interiors, 100, 135–156, 10.1016/S0031-9201(96)03236-0, physical and Chemical Evolution of the Earth, 1997.

Tackley, P.J., 2000. Mantle Convection and Plate Tectonics: Toward an Integrated Physical and Chemical Theory. Science 288, 2002–2007. https://doi.org/10.1126/science.288.5473.2002.

Tackley, P.: Mantle Geochemical Geodynamics, Treatise on Geophysics, pp. 437–505, 10.1016/b978-044452748-6.00124-3, 2007.

Torsvik, T.H., Smethurst, M.A., Burke, K., Steinberger, B., 2006. Large igneous provinces generated from the margins of the large low-velocity provinces in the deep mantle. Geophys. J. Int. 167, 1447–1460. https://doi.org/10.1111/j.1365-246x.2006.03158.x.

Torsvik, T.H., Steinberger, B., Cocks, L.R.M., Burke, K., 2008. Longitude: Linking Earth's ancient surface to its deep interior. Earth Planet. Sci. Lett. 276, 273–282. https://doi.org/10.1016/j.epsl.2008.09.026.

Torsvik, T.H., Burke, K., Steinberger, B., Webb, S.J., Ashwal, L.D., 2010. Diamonds sampled by plumes from the core–mantle boundary. Nature 466, 352–355. https://doi.org/10.1038/nature09216.

Trampert, J., 2004. Probabilistic Tomography Maps Chemical Heterogeneities Throughout the Lower Mantle. Science 306, 853–856. https://doi.org/10.1126/science.1101996.

Trampert, J., Vacher, P., Vlaar, N., 2001. Sensitivities of seismic velocities to temperature, pressure and composition in the lower mantle. Phys. Earth Planet. In. 124, 255–267. https://doi.org/10.1016/S0031-9201(01)00201-1.

van Hinsbergen, D.J.J., Steinberger, B., Doubrovine, P.V., Gassmöller, R., 2011. Acceleration and deceleration of India-Asia convergence since the Cretaceous: Roles of mantle plumes and continental collision. J. Geophys. Res. 116. https://doi.org/10.1029/2010jb008051.

Weis, D., Garcia, M.O., Rhodes, J.M., Jellinek, M., Scoates, J.S., 2011. Role of the deep mantle in generating the compositional asymmetry of the Hawaiian mantle plume. Nat. Geosci. 4, 831–838. https://doi.org/10.1038/ngeo1328.

Weller, M.B., Lenardic, A., 2012. Hysteresis in mantle convection: Plate tectonics systems. Geophys. Res. Lett. 39. https://doi.org/10.1029/2012GL051232.

White, W.M., 1985. Sources of oceanic basalts: Radiogenic isotopic evidence. Geology 13, 115–118. https://doi.org/10.1130/0091- 7613(1985)13<115:SOOBRI>2.0.CO;2.

White, W.: Probing the Earth's Deep Interior Through Geochemistry, Geochemical Perspectives, pp. 95–251, 10.7185/geochempersp.4.2, 2015.

Whittaker, J.M., Afonso, J.C., Masterton, S., Müller, R.D., Wessel, P., Williams, S.E., Seton, M., 2015. Long-term interaction between mid-ocean ridges and mantle plumes. Nat. Geosci. 8, 479–483. https://doi.org/10.1038/ngeo2437.

Williams, C.D., Li, M., McNamara, A.K., Garnero, E.J., van Soest, M.C., 2015. Episodic entrainment of deep primordial mantle material into ocean island basalts. Nat. Commun. 6. https://doi.org/10.1038/ncomms9937.

Xu, W., Lithgow-Bertelloni, C., Stixrude, L., Ritsema, J., 2008. The effect of bulk composition and temperature on mantle seismic structure. Earth Planet. Sci. Lett. 275, 70–79. https://doi.org/10.1016/j.epsl.2008.08.012.

Yoshida, M., Santosh, M., 2011. Supercontinents, mantle dynamics and plate tectonics: A perspective based on conceptual vs. numerical models. Earth Sci. Rev. 105, 1–24. https://doi.org/10.1016/j.earscirev.2010.12.002.

Yoshida, M., Iwase, Y., Honda, S., 1999. Generation of plumes under a localized high viscosity lid in 3-D spherical shell convection. Geophys- Ical Research Letters 26, 947–950. https://doi.org/10.1029/1999GL900147.

Zaroli, C., Koelemeijer, P., Lambotte, S., 2017. Toward seeing the Earth's interior through unbiased tomographic lenses. Geophys. Res. Lett. 44, 11399–11408. https://doi.org/10.1002/2017GL074996.

Zhang, N., Li, Z.-X., 2018. Formation of mantle "lone plumes" in the global downwelling zone — A multiscale mod- elling of subduction-controlled plume generation beneath the South China Sea. Tectonophysics 723, 1–13. https://doi.org/10.1016/j.tecto.2017.11.038.

Zhang, N., Zhong, S., Leng, W., Li, Z.-X., 2010. A model for the evolution of the Earth's mantle structure since the Early Paleozoic. J. Geophys. Res. 115. https://doi.org/10.1029/2009jb006896.

Zhong, S., Liu, X., 2016. The long-wavelength mantle structure and dynamics and implications for large-scale tectonics and volcanism in the Phanerozoic. Gondw. Res. 29, 83–104. https://doi.org/10.1016/j.gr.2015.07.007.

Zhong, S., Rudolph, M.L., 2015. On the temporal evolution of long-wavelength mantle structure of the Earth since the early Paleozoic. Geochem. Geophys. Geosyst. 16, 1599–1615. https://doi.org/10.1002/2015gc005782.